

# Late Pleistocene to Holocene temporal succession and magnitudes of highly-explosive volcanic eruptions in west-central Nicaragua

S. Kutterolf<sup>a,\*</sup>, A. Freundt<sup>a,b</sup>, W. Pérez<sup>a</sup>, H. Wehrmann<sup>a</sup>, H.-U. Schmincke<sup>a,b</sup>

<sup>a</sup> SFB 574 at Kiel university/ IFM-GEOMAR, Wischhofstr. 1-3,  
Gebäude 8A/213, 24148 Kiel, Germany

<sup>b</sup> IFM-GEOMAR/ Research Division 4/Dynamics of the Ocean Floor, Wischhofstr. 1-3,  
Gebäude 8E/208, 24148 Kiel, Germany

Received 2 June 2006; received in revised form 20 February 2007; accepted 23 February 2007  
Available online 21 March 2007

## Abstract

The stratigraphic succession of widespread tephra layers in west-central Nicaragua was emplaced by highly explosive eruptions from mainly three volcanoes: the Chiltepe volcanic complex and the Masaya and Apoyo calderas. Stratigraphic correlations are based on distinct compositions of tephra. The total tephra combine to a total on-shore volume of about 37 km<sup>3</sup> produced during the last ~60 ka. The total erupted magma mass, including also distal volumes, of 184 Gt (DRE) distributes to 84% into 9 dacitic to rhyolitic eruptions and to 16% into 4 basaltic to basaltic–andesitic eruptions. The widely dispersed tephra sheets have up to five times the mass of their parental volcanic edifices and thus represent a significant albeit less obvious component of the arc volcanism. Eruption magnitudes ( $M = \log_{10}(m) - 7$  with  $m$  the mass in kg), range from  $M = 4.1$  to  $M = 6.3$ . Most of the eruptions were dominantly plinian, with eruption columns reaching variably high into the stratosphere, but minor phreatomagmatic phases were also involved. Two phreatomagmatic eruptions, one dacitic and one basaltic–andesitic, produced mostly pyroclastic surges but also fallout from high eruption columns. Comparison of fallout tephra dispersal patterns with present-day, seasonally changing height-dependant wind directions suggests that 8 eruptions occurred during the rainy season while 5 took place during the dry season. The tephra succession documents two major phases of erosion. The first phase, >17 ka ago, appears to be related to tectonic activity whereas the second phase may have been caused by wet climatic conditions between 2 to 6 ka ago. The Apoyo caldera had two large plinian, caldera-forming eruptions in rapid succession about 24 ka ago and should be considered a silicic volcano with long repose times. Three highly explosive basaltic eruptions were generated at the Masaya Caldera within the last 6 ka. Since then frequent but small eruptions and lava effusion were largely limited to the caldera interior. The dacitic Chiltepe volcanic complex experienced six plinian eruptions during the last 17 ka and seems to be an accelerating system in which eruption magnitude increased while the degree of differentiation of erupted magma decreased at the same time. We speculate that the Chiltepe system might produce the next large-magnitude silicic eruption in west-central Nicaragua.

© 2007 Elsevier B.V. All rights reserved.

**Keywords:** tephrostratigraphy; Nicaragua; plinian eruptions; distribution; eruption parameter

\* Corresponding author. Tel.: +49 431 600 2565; fax: +49 431 600 2915.  
E-mail address: [skutterolf@ifm-geomar.de](mailto:skutterolf@ifm-geomar.de) (S. Kutterolf).

## 1. Introduction

The volcanic front of Nicaragua is part of the Central American Volcanic Arc (CAVA), an area with one of the highest densities of active volcanoes in the world. The Quaternary explosive eruptive activity ranged in style from strombolian through violently surtseyan to plinian and included also ignimbrite-forming eruptions. Large-magnitude eruptions in west-central Nicaragua occurred from both felsic as well as mafic volcanoes. These eruptions were typically separated by long periods of time. Assessing the hazard from this kind of activity in this densely inhabited area requires the knowledge of how the style, intensity, and magnitude of eruptions evolved with time at each of the contributing volcanoes. This paper focuses on field aspects of the tephra succession, particularly on stratigraphic relationships and tephra dispersal characteristics, which allow determining dynamic parameters of the eruptions. Additional constraints on tephra dispersal are derived from the Pacific offshore tephra record which we discuss in separate contributions (Kutterolf et al., submitted for publication-a,b). In previous publications, we used this data set to assess future hazards from large

eruptions and to constrain the temporal evolution of the smaller-scaled volcanism in and near Managua (Freundt et al., 2006a), to investigate petrogenetic relationships within and between volcanic systems, and to estimate the individual and long-term cumulative fluxes of volatiles into the stratosphere by these eruptions. Toward the end of this paper, we draw general conclusions in regard to the morphological evolution of west-central Nicaragua in response to tectonic and/or climatic events. Finally we estimate the size of magmatic systems, document seasonal variations in tephra dispersal, and discuss future volcanic hazards.

## 2. Geological setting of western Nicaragua

Nicaragua forms the central part of the Central America Isthmus, between the Caribbean coast and the Central American trench on the Pacific side. The Central American Volcanic Arc (CAVA) formed in response to subduction of the Cocos plate beneath the Caribbean plate since the late Cretaceous. The volcanic front shifted westward with time and assumed its present position about 8 Ma ago (Ehrenborg, 1996). Nicaragua can be divided, from west to east, into the Pacific Coastal Plain, the Nicaragua

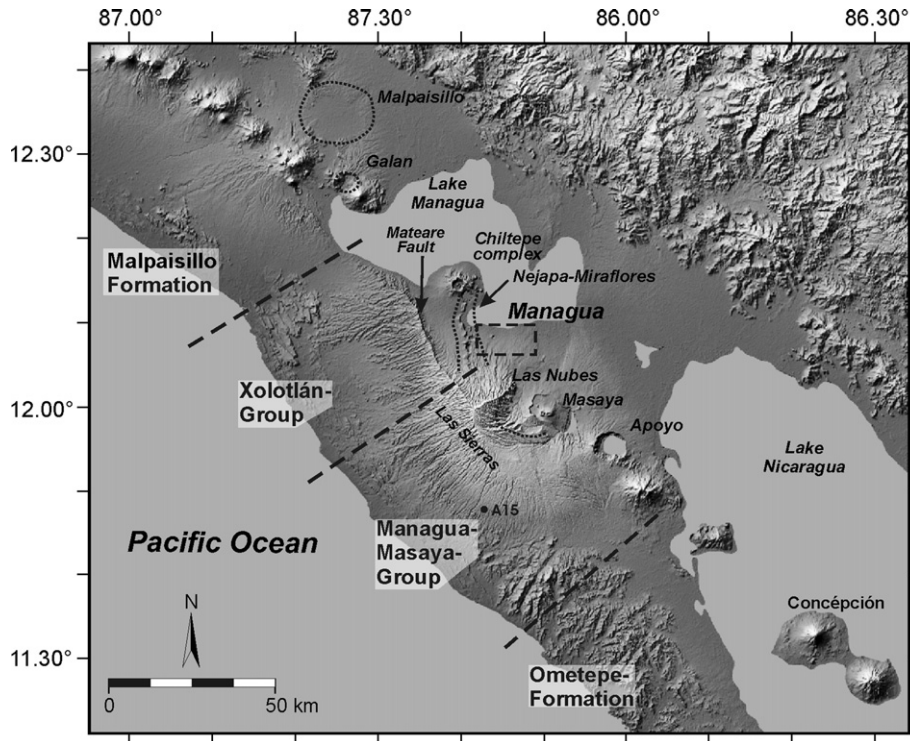


Fig. 1. Map of western Nicaragua and the adjacent Pacific showing lakes Managua and Nicaragua within the NW–SE trending Nicaraguan depression and the arc volcanoes. Lines schematically indicate the areas between the volcanic front and the coast that are characterized by different tephrostratigraphic successions.

Depression, the Interior Highland, and the Atlantic Coastal Plain (Weyl, 1980). The NW–SE trending, ~45-km-wide Nicaragua Depression is filled with approximately 6 km of volcanoclastic and marine sediments (McBirney and Williams, 1965; Weyl, 1980). The depression has been interpreted as a tectonic graben that probably began to subside in the Late Miocene (McBirney and Williams, 1965; Dengo et al., 1970). Since the Early Pleistocene this depression contains two large lakes, Lake Nicaragua and Lake Managua. The Nicaraguan volcanic front lies within, and to the west of the Nicaraguan Depression and crosses both lakes. It comprises at least 12 major volcanic complexes that have been active during the Holocene, including 6 presently active volcanoes.

West of Managua, an offset in the NW–SE striking volcanic front between Chiltepe peninsula and Masaya caldera is marked by the Nejapa–Miraflores lineament, an N–S-trending fault zone straddled by numerous cinder cones and tuff-rings, many of which lie within Managua's city limits (Fig. 1). Another zone of scoria cones developed NW of Granada (Ui, 1972; Walker, 1984).

Highly explosive large-magnitude eruptions (VEI up to 5) that produced widely dispersed tephra sheets across west-central Nicaragua during the past few ten thousand years mainly occurred at three volcanoes: Apoyo Caldera, Masaya Caldera, and the Chiltepe volcanic complex. Bice (1985) first studied this succession of widespread tephra sheets in the wider Managua area, building on earlier stratigraphic and geochemical studies cited therein (and partly reviewed in Weyl, 1980). According to Bice, the Managua Sequence comprises seven widespread basaltic and rhyodacitic tephra layers (Fig. 2) overlying the Las Sierras Group, an up to 680 m thick sequence of mafic Tertiary to Quaternary volcanoclastic deposits. Bice (1985) and Sussman (1985) mapped the major dacitic pyroclastic deposits of the Managua Sequence, estimated tephra volumes, and discussed eruption processes. Williams (1983a,b) recognized that the widespread basaltic fallout tephra were produced by plinian eruptions from Masaya Caldera. These plinian basaltic fallouts were studied in more detail by Pérez and Freundt (2006) and Wehrmann et al. (2006). The Czech Geological Survey in collaboration with the Instituto Nicaragüense de Estudios Territoriales (INETER), has produced new geological maps since the 1990's (Hradecky, 2001) that identify stratigraphic groups but not individual tephra layers.

### 2.1. Apoyo Caldera

The Apoyo Caldera, 35 km southeast of Managua, is a 6.5-km-diameter, ~600 m deep circular subsidence structure (Sussman, 1985). The oldest rocks exposed

consist of pyroclastic and volcanoclastic deposits of the Las Sierras Formation (McBirney and Williams, 1965). These rocks are overlain by a series of flat to gently dipping basaltic to andesitic lavas that extruded from Apoyo volcano over a relatively short time span and form a broad shield (Sussman, 1985). Several small rhyodacite domes peripheral to the present caldera and arranged along N–S trending normal faults were dated at  $90 \pm 40$  ka (Williams, 1972). The Apoyo caldera formed ~24 ka ago by two plinian eruptions producing the Lower and Upper Apoyo Tephra which were separated by only a short period of time (order of

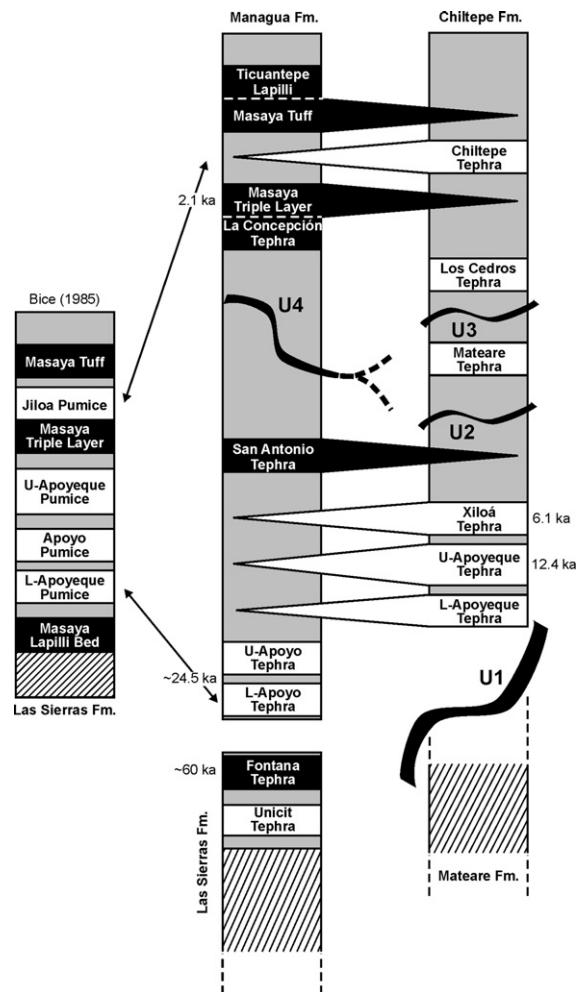


Fig. 2. Composite stratigraphic successions of Late Pleistocene/Holocene tephra from highly explosive eruptions in west-central Nicaragua. Left column shows the tephra sequence after Bice (1985); right columns summarize the results of this study, regarding the Chiltepe and Managua Formations. Arrows indicate major differences with respect to Bice's (1985) stratigraphy. Black: mafic tephra, white: felsic tephra; pointed boxes indicate observed intercalations between the two formations. Major erosional unconformities are indicated as U1 to U4.

$10^2$  years). We found four rhyodacitic pumice fallout layers of unknown age that are separated by paleosols and other volcanoclastic sediments and hence, significantly pre-date the 24-ka-tephras, indicating that plinian eruptions already occurred prior to caldera formation.

## 2.2. Masaya Caldera

The Masaya Caldera and its eruptive products were studied by [McBirney \(1955a, 1956\)](#), [Ui \(1972\)](#), [Williams \(1983a\)](#), [Wehrmann et al. \(2006\)](#), and [Pérez and Freundt \(2006\)](#). Within the caldera, a post-collapse volcanic complex (Santiago–Masaya volcano) has been active frequently in historic times. All products of the post-caldera Masaya volcanoes are basaltic or basaltic–andesitic ([McBirney, 1956; Ui, 1972; Williams, 1983a; Walker et al., 1993](#)) containing mostly olivine and augite crystals.

The long axis of the shallow (100–300 m), 6 by 11 km oval Masaya Caldera lies parallel to the volcanic front. [McBirney \(1956\)](#) suggested that the caldera formed by a series of coalescing collapses in response to a large-scale “recession of magma”. [Bice \(1985\)](#) and [Williams \(1983a\)](#) concluded that the Masaya Caldera formed as a result of one or several explosive basaltic eruptions. [Bice and Williams](#) studied three widespread basaltic tephra that they attributed to Masaya Caldera: the Fontana Tephra and the Masaya Triple Layer, both of plinian dispersal, and the Masaya Tuff, a huge phreatomagmatic surge deposit. [Pérez and Freundt \(2006\)](#) identified additional widespread basaltic tephra deposits that are discussed below.

## 2.3. Chiltepe volcanic complex

The 11 km-wide Chiltepe Peninsula, 6 km north of Managua on the western shore of Lake Managua, contains several scoria cones and tuff-rings, the morphologically prominent central Apoyeque stratocone (including several domes and lavas), and the Xiloá maar. We suggest additional buried plinian vents east of Mateare ([Freundt et al., 2006b](#)) and in Lake Managua southeast of the peninsula. [McBirney \(1955a\)](#) speculated about the possible existence of another source vent beneath Lake Managua that might have erupted some of the pumice layers exposed in the city of Managua. [Bice \(1985\)](#), however, did not see the necessity to postulate any hidden vents in order to explain the origin of the Managua Sequence.

Apoyeque stratovolcano has a nearly circular, lake-filled, steep-walled crater (2.75 km in diameter and 250 m deep) that is occupied by a lake. The lower part of the Apoyeque stratovolcano is composed of amphibole- and pyroxene–andesite ([Sapper, 1925; Williams, 1952a;](#)

[McBirney, 1955a](#)) and basaltic lava flows ([Kuang, 1971](#)). [Bice \(1985\)](#) implied that the dacitic plinian Lower and Upper Apoyeque tephra were erupted from Apoyeque volcano.

Laguna Xiloá fills a circular maar crater with scalloped margins that is 2.5 km in diameter. Its rim rises from just above the level of Lake Managua in the southeast to 220 m on the northern side where it intersects the flank of Apoyeque stratovolcano ([Bice, 1985](#)). The dacitic Xiloá Tephra, comprising pyroclastic surge and fallout deposits, was erupted during violent phreatomagmatic eruption from this crater.

## 3. Methods and approaches

### 3.1. Fieldwork data

We studied ~230 outcrops between Nagarote in the north and Granada in the south in order to establish stratigraphic relations and construct isopach and isopleth maps of major widespread tephra layers in Central Nicaragua. Field correlations are based on modal and chemical compositions, textures of pumices, sedimentary structures, relative position, radiometric ages, occurrence of unconformities and the nature of intercalated sediments. Selected detailed stratigraphic columns of complex tephra successions are shown in Supplementary Figs. 1 to 5. We also obtained 5 new radiocarbon dates. Since most tephra were dispersed westerly toward the Pacific coast, only 30–40 km west of the volcanic front, we refer also to 47 marine gravity cores we collected on the continental slope and the incoming plate offshore Nicaragua ([Fig. 1](#)). In [Kutterolf et al. \(submitted for publication-b\)](#) we show that many of the ash layers in these cores are distal equivalents of tephra on land discussed here. Details on the coring method, core profiles, and analytical and correlation techniques are reported in [Kutterolf et al. \(submitted for publication-b, 2007\)](#).

### 3.2. Chemical analyses

In order to facilitate on-land stratigraphic correlations, bulk-rock concentrations of major and trace elements were determined by X-ray fluorescence analysis with an automated Philips X'Unique PW 1480 XRF spectrometer, using glass pellets made from finely ground sample powder mixed with lithium borate as fluxing agent. A CAMECA SX 50 wavelength-dispersive electron microprobe (EMP) was used for spot analyses of major elements in minerals and glasses. EMP analyses were conducted at 15 kV accelerating voltage and a beam

current of 10 nA; only 6 nA was used for felsic glass. The beam was defocused to 5  $\mu\text{m}$  to minimize analytical Na-loss. International natural and synthetic glass and mineral standards were used for calibration. Standard deviation is less than 0.5% for major elements and <3% for minor elements. All analytical data presented below were normalized to anhydrous compositions.

### 3.3. Radiocarbon dating

Samples of charcoal and carbon-bearing soil and sediment were analyzed at the Leibniz Laboratory for Radiometric Dating and Isotope Research at Kiel University. The samples were checked and mechanically cleaned under the microscope, afterwards sieved, and the dark organic-looking material <250  $\mu\text{m}$  was selected for further treatment. Conventional  $^{14}\text{C}$  ages were calculated following procedures described by Stuiver and Polach (Stuiver and Polach, 1977) with a  $\delta^{13}\text{C}$  correction for isotopic fractionation based on the  $^{13}\text{C}/^{12}\text{C}$  ratio measured by the Accelerator Mass Spectrometer (AMS) system simultaneously with the  $^{14}\text{C}/^{12}\text{C}$  ratio. The alkali extraction of the organic fraction (humic acid fraction) was precipitated with HCl, washed and dried, and afterwards also measured by the AMS-system. In addition to analytical uncertainty, there is some uncertainty due to possible sample contamination. Thus, the analyzed solid fraction of soil and sediment samples may be mixed with older carbon particles. The humic acid fraction on the other hand, can be easily contaminated by younger groundwater-carbon. The new  $^{14}\text{C}$  ages are listed in Table 1, where such uncertainties are qualitatively addressed.

### 3.4. Bulk-density measurements

Batches of 10–15 lapilli of pre-determined bulk weight were mixed with loosely packed, ideally sorted coarse sand of known bulk density in a fixed-volume container and weighed. This allowed calculating their bulk volume and thereby their average bulk density with an uncertainty  $\leq 5\%$  deduced from repeated measurements (5 per sample, 3 samples of different distances to the vent per tephra). The measured density of powdered bulk rock (5 pumice clasts) allowed to estimate pumice porosity.

### 3.5. Determination of eruption parameters

Total tephra volumes were obtained by fitting straight-line segments to data on plots of  $\ln$  [isopach thickness] versus square-root [isopach area] following the methods of Pyle (1989) and Fierstein and Nathenson (1992). Tephra volumes were converted to erupted magma masses using measured pumice–lapilli bulk densities of 400–700  $\text{kg}/\text{m}^3$  for felsic and 800–900  $\text{kg}/\text{m}^3$  for mafic tephtras over proximal and medial ranges per tephra unit, ash-particle densities of 2100–2400  $\text{kg}/\text{m}^3$  over distal ranges (<20 cm thickness), and allowing for 50 vol.% interparticle pore space and lithics (which commonly constitute a minor component only).

Maximum pumice (MP) and maximum lithic (ML) data are the average diameter of the five largest clasts, with the average of three axes determined for each clast. Cross-range half-widths of MP- and ML-isopleths were compared with eruption-column modeling results of Carey and Sparks (1986) and Wilson and Walker (1987). Such

Table 1

$^{14}\text{C}$  age data of Nicaraguan Tephtras; MTL = Masaya Triple Layer, XT = Xiloá Tephra, UAq = Upper Apoyeque tephra, UAT = Upper Apoyo Tephra and LAT = Lower Apoyo Tephra

Tephra	Sample	Depth below surface (m)	Date BP	Error	$\delta^{13}\text{C}$ (‰)	LAB #	UTM		Date BP	Error	$\delta^{13}\text{C}$ (‰)	Comments
							E	N				
MTL	Plant remains	2.5	2120	$\pm 120$	$-34.23 \pm 0.21$	KIA-18584	0574642	1332107	–	–	–	Critical C-content causes large error
XT	charcoal in tephra	4	6105	$\pm 30$	$-28.42 \pm 0.11$	KIA-18579	0572647	1349654	5955	$\pm 30$	$-25.14 \pm 0.08$	Alkali date reliable, humic date contaminated by young stuff and less reliable
UAq	underlying paleosol	5	12,400	$\pm 100$	$-20.89 \pm 0.12$	KIA-24437	0567228	1341302	–	–	–	Little organic, critical C-content causes large error
UAT	charcoal in tephra	20	–	–	–	KIA-21013	602467	1314190	24650	$\pm 120$	$-24.25 \pm 0.14$	All dissolved to humic, charcoal already strongly altered but still reliable
LAT	underlying paleosol	3	23,890	$\pm 240$	$-24.07 \pm 0.06$	KIA-21014	597298	1318318	–	–	–	Enough C, reliable

comparisons allowed estimating eruption column heights and magma discharge rates which were cross-checked for consistency against model curves of Woods (1988).

#### 4. West-central Nicaraguan tephrostratigraphy

We distinguish four volcanoclastic successions in west-central Nicaragua that differ in their stratigraphy and volcanic sources. From north to south these are (Fig. 1):

- (1) The Malpaisillo Formation, exposed in the plains between Nagarote, La Paz Centro, El Hoyo and

Momotombo, comprises several dacitic pumice fallout and ignimbrite units. Van Wyk de Vries (1993) proposed that this succession is related to the Monte Galan or Malpaisillo calderas (Fig. 1). Our stratigraphic correlations confirm an origin in the Malpaisillo caldera. These dacitic rocks are compositionally distinct from those of the Xolotlán Group.

- (2) The Xolotlán Group between Nagarote and Managua comprises the Chiltepe Formation and the underlying Mateare Formation, separated from each other by a large regional unconformity (U1 in Figs. 2 and 3). The detailed stratigraphy

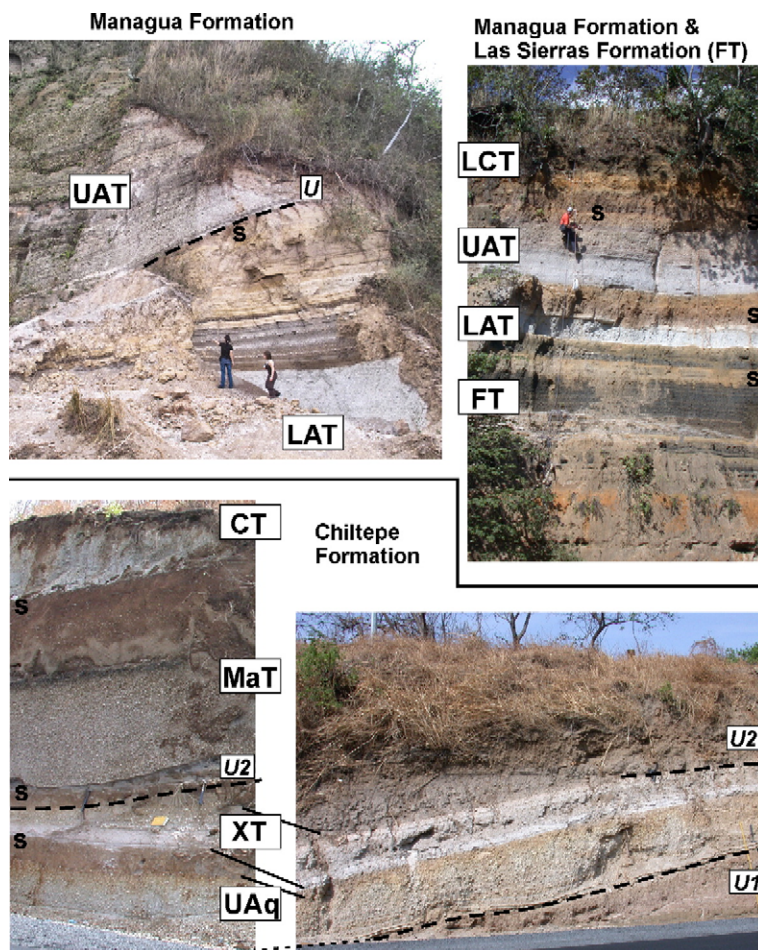


Fig. 3. Photographs showing tephra sequences of the Managua and Las Sierras (top) and Chiltepe Formation (bottom). LCT = La Concepción Tephra, UAT = Upper Apoyo Tephra, LAT = Lower Apoyo Tephra, FT = Fontana Tephra, CT = Chiltepe Tephra, MaT = Mateare Tephra, XT = Xiloá Tephra, UAq = Upper Apoyeque Tephra. s = intercalated paleosols and sediments. U1 and U2 are unconformities discussed in the text; U in top-left photo is an unconformity between LAT and UAT at the Apoyo crater rim. Top left: Loc. A003, Apoyo caldera rim at Diria (UTM E0603646, N1315040) showing white LAT pumice fall overlain by brown stratified phreatomagmatic fall, and UAT-1 stratified pumice fall above unconformity U. Top right: Loc. A55 in San Marcos (E0586466, N1318229) with conformable succession from FT to UAT; the unconformity (U4 in text) below LCT cannot be seen here. Bottom left: Loc. A96 at road Mateare–Nagarote (E0558032, N1355523) with succession from UAq to CT; note thin black top of zoned MaT and unconformity U2 cutting through XT. Bottom right: Loc. A116 at road Mateare–Nagarote (E0556576, N1356425) where UAq and XT overlie unconformity U1 on top of the Mateare Formation, and XT is cut by U2.

and compositional evolution of the Mateare Formation will be presented elsewhere. The Mateare Formation forms the morphology west of Lake Managua which has previously been considered as the northern part of the Las Sierras Formation (Van Wyk de Vries, 1993). However, the Las Sierras Formation is mainly of mafic to intermediate composition, while the Mateare Formation is dominated by felsic tephra.

(3) The Managua–Masaya Group between Managua, Jinotepe and Granada includes the younger Managua Formation (Managua Sequence of Bice, 1985) and the older Las Sierras Formation (McBirney and Williams, 1965). There is no unconformity south of Managua to define the boundary between these two formations. We place the boundary between the Las Sierras and Managua formations between the Fontana and Lower Apoyo tephra (Fig. 2) for the following reasons:

- (a) Wehrmann et al. (2006) showed that the Fontana Tephra was most likely not erupted from the Masaya caldera but from a vent some kilometers to the NW inside the older Las Nubes Caldera (Sebesta, 1997). Kutterolf et al. (submitted for publication-b) use stratigraphic relationships in offshore sediment cores to constrain an age of 55–68 ka for the Fontana Tephra, older than the 30–40 ka estimated by Bice (1985), Williams (1983a) and Wehrmann et al. (2006).
- (b) The Las Sierras Formation has not yet been studied in detail and its internal stratigraphy, rock compositions and source vents remain largely unknown. Girard and van Wyk de Vries (2005) interpreted the Las Sierras edifice as a mafic to intermediate ignimbrite shield. We have obtained a radiocarbon date of ~34 ka from charcoal in a basaltic–andesitic ignimbrite at Boquita Cazares west of Diriamba (locality A15 in Figs. 1 and 4A), which appears to be part of the Las Sierras Formation.
- (4) The Ometepe Formation is a sequence of basaltic to rhyolitic pyroclastic deposits derived from vents of Concepción volcano on the island of Ometepe in Lake Nicaragua. Borgia and van Wyk de Vries (2003) studied a basaltic to dacitic tephra succession ranging from recent to >3 ka in age, that includes the prominent dacitic Tierra Blanca Tephra erupted 2720±60 years BP. An additional tephra section of dacitic and dacite–andesite mixed compositions can be chemically correlated with ash beds in the Pacific slope sediment sequence, which are *c.* 19 ka old as

estimated from sediment accumulation rates (Kutterolf et al., 2007, submitted for publication-b).

Radiometric dates show that all four successions largely overlap in time. So far we only found geologic evidence for interfingering stratigraphies between the Chiltepe and the Managua formations, which are the focus of this paper. Our revised and extended composite stratigraphy of these two formations, including several newly described dacitic and basaltic tephra layers, is compiled in Fig. 2. Table 2 summarizes modal compositions, depositional characteristics, and pumice bulk densities and porosities of all the tephra units. The tephra units of the Chiltepe and Managua formations are described below.

## 5. The Chiltepe Formation

The Chiltepe Formation is defined as a sequence of volcanoclastic deposits that is separated from the underlying Mateare Formation by a regional erosional unconformity older than ~17 ka, the estimated age for Lower Apoyeque Tephra (Kutterolf et al., submitted for publication-b). The unconformity is characterized by an amplitude that exceeds 50 m, reflecting the paleo-drainage system directed toward Lake Managua (Fig. 3). The six tephra units of the Chiltepe Formation were all emplaced within the last 17 ka by highly explosive eruptions from vents on or near Chiltepe peninsula.

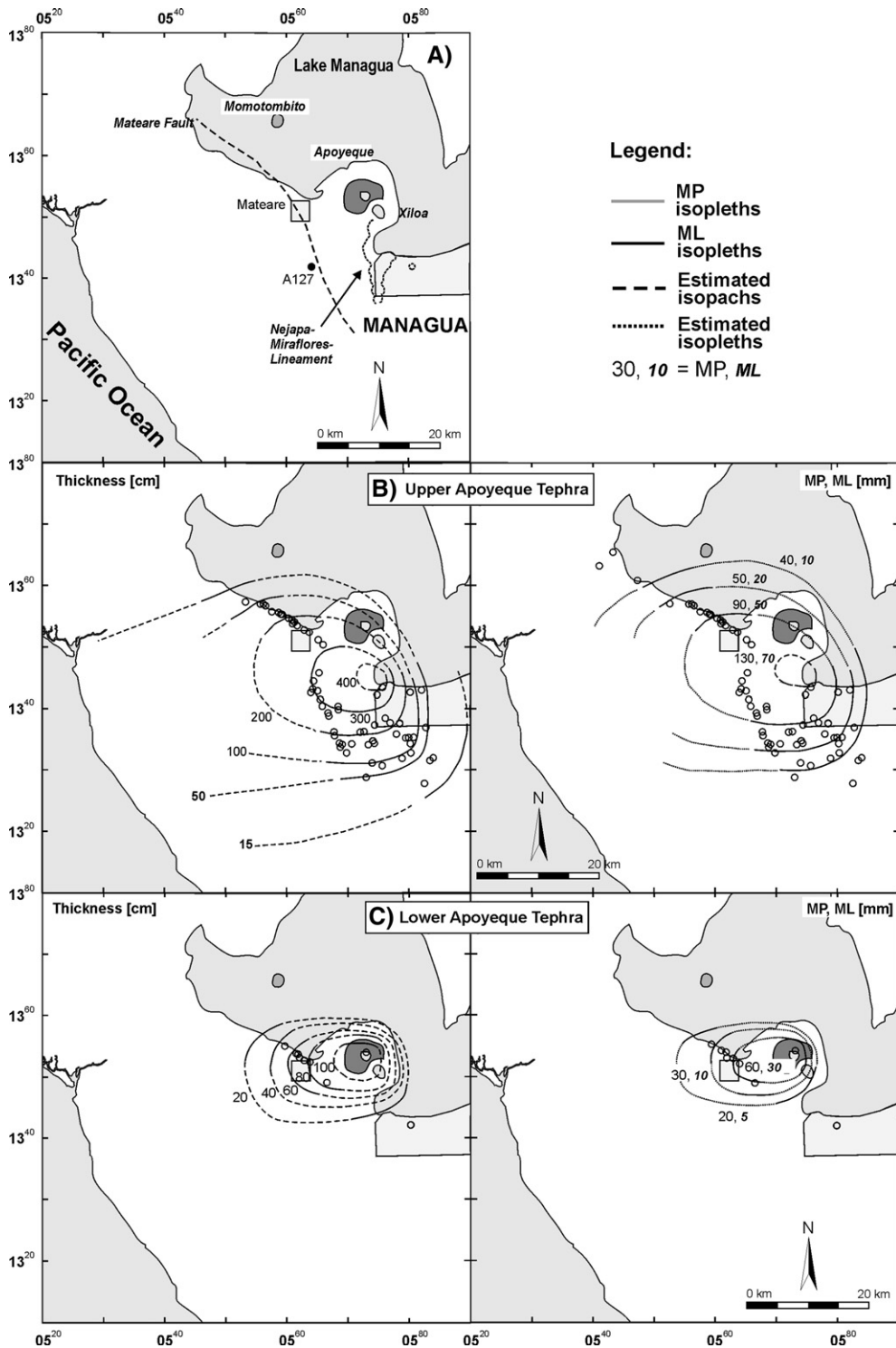
### 5.1. Lower Apoyeque Tephra (LAq)

The ~17 ka old dacitic plinian Lower Apoyeque Tephra originally mantled the U1 unconformity (Fig. 2), separated only by a thin layer of tuffaceous sediment. However, it was already largely eroded prior to emplacement of the overlying Upper Apoyeque Tephra. For this reason we only found the LAq at 12 outcrops near Mateare where it forms a single inversely graded massive pumice fallout bed that reaches up to 130 cm in thickness. The deposit south of Managua that Bice (1985) reported as the Lower Apoyeque Pumice is actually the Lower Apoyo Tephra (Fig. 2) as established by compositional comparisons.

Near the present shore of Lake Managua in Mateare, the LAq directly overlies lacustrine sediments, which is evidence for a higher lake level ~17 ka ago. The few available outcrops indicate a distribution of the fallout fan toward the WNW from a vent site on the Chiltepe peninsula (Fig. 4D,F). Rough estimates limited by the available data suggest an erupted tephra volume of approximately 1.0 km<sup>3</sup> corresponding to ~1.2 × 10<sup>11</sup> kg

of magma (Fig. 5), a magma discharge rate of 2 to  $3 \times 10^7$  kg/s (Fig. 6) and a column height of 20–23 km at 10–20 m/s wind speed (Figs. 7 and 8).

Compositional characteristics of the Lower Apoyeque rhyodacitic pumice include the presence of abundant amphibole phenocrysts (as well as pl, opx and cpx, ti-mt,



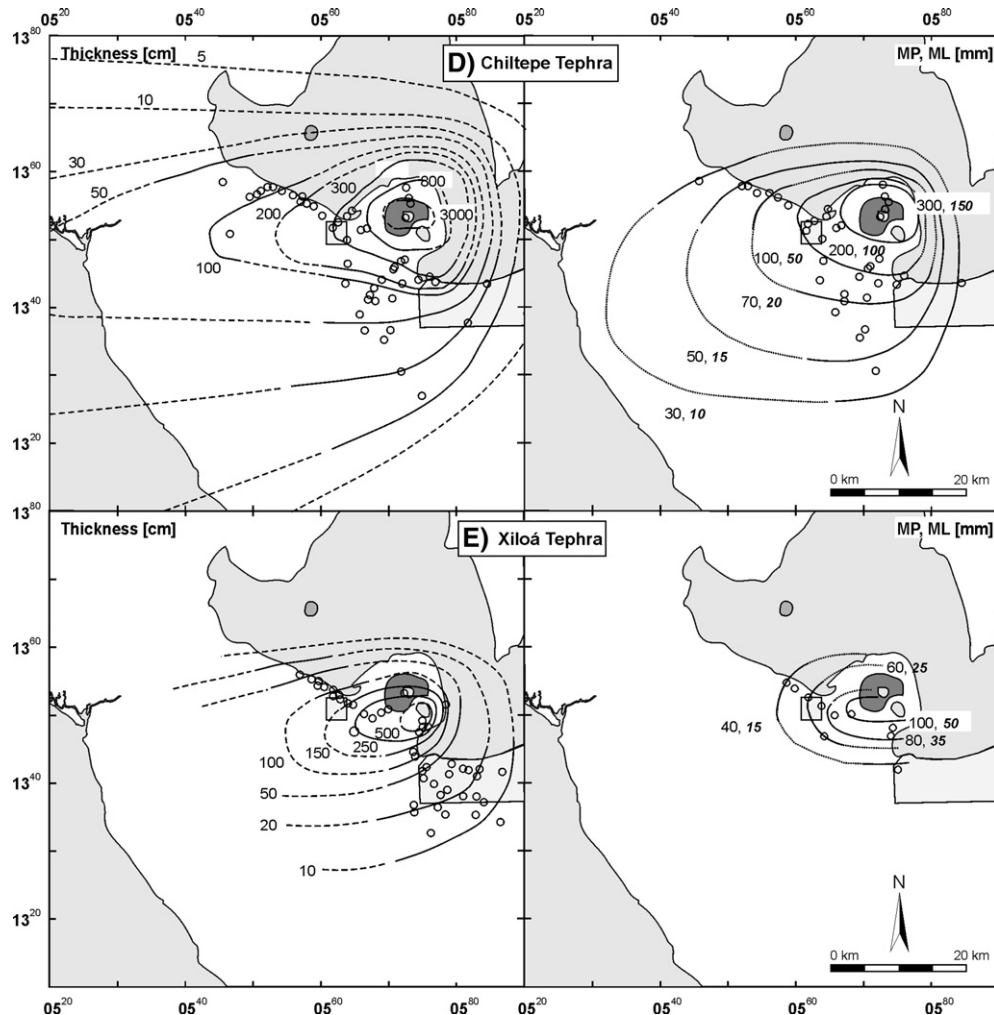


Fig. 4. A) Location map of the area north of Managua. Note Nejapa–Miraflores zone at western limit of Managua. Locality A127 on top of the Mateare Fault scarp is addressed in the text. Isopach and isopleth maps for the Upper Apoyeque Tephra (B) and the Lower Apoyeque Tephra (C). Solid lines are well-constrained, dashed lines are estimated. MP, ML are maximum pumice and lithic-clast sizes in mm as defined in the text and isopach thickness is given in cm. Unfilled circles show outcrop locations. ML-isopleths are labeled with smaller italic numbers for lithics where shown together with the gray MP-isopleths. For isopach and isopleth maps of the mafic tephra see Pérez and Freundt (2006) and Wehrmann et al. (2006); for those of the Mateare Tephra see Freundt et al. (2006b). Isopach and isopleth maps for the Chiltepe (D) and Xiloá (E) Tephra. F) Location map of the area south of Managua. A15 is a location addressed in the text. G) Isopach and isopleth maps for the Upper Apoyo Tephra. H) Isopach and isopleth maps for the Lower Apoyo Tephra.

ap; Table 2), and a highly evolved bulk-rock composition with 71 wt.% SiO<sub>2</sub> and the highest concentrations in K<sub>2</sub>O and Zr but lowest contents in TiO<sub>2</sub> and Sr compared to the other evolved tephra (Fig. 9A,C,D). The matrix glass is depleted in FeO, CaO and enriched in silica (Fig. 10A,B,E).

### 5.2. Upper Apoyeque Tephra (UAq)

The age of the dacitic plinian Upper Apoyeque Tephra is constrained by a <sup>14</sup>C age of 12,400±100 years BP

obtained on the immediately underlying thin paleosol (Table 1, Fig. 3) that caps tuffaceous sediment on top of the LAq. The reversely graded UAq is identical to the Upper Apoyeque Pumice described by Bice (1985). This tephra is commonly the first pyroclastic deposit on top of the 17-ka regional unconformity U1 because the LAq has been extensively eroded and is generally absent. The UAq is a coarse pumice lapilli fallout deposit that is reversely graded across the weakly stratified lower half but massive and coarse-grained in its upper half. A basal fallout set of three yellow fine-grained ash layers separated by coarse-

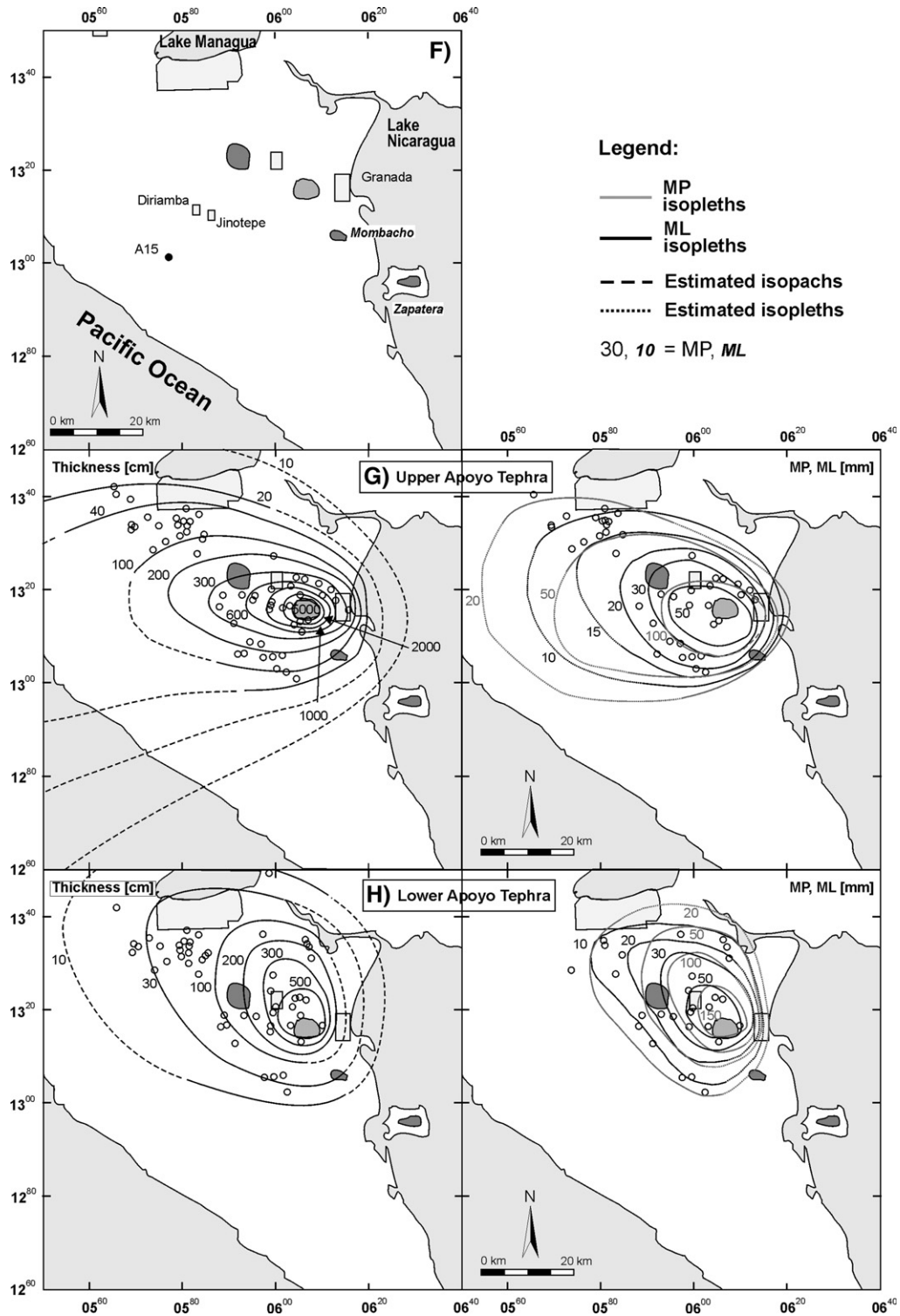


Fig. 4 (continued).

ash layers is <15 cm thick in proximal outcrops and merges to a single thin ash bed in distal sections (Fig. S1). The fine ash beds locally form vesiculated tuffs. On slopes

near and inclined toward Lake Managua the ash package slumped prior to the deposition of the overlying pumice fallout. These features suggest wet emplacement.

Bice (1985) observed a northward increase in thickness of the UAq in and south of Managua. Therefore he proposed Apoyeque volcano as the source vent. However, the deposit reaches a maximum observed thickness of 400 cm at the southwestern bay of Lake Managua between Chiltepe peninsula and Managua city. From here on, the thickness of the tephra decreases rapidly to the east, less rapidly to the south, and only very gradually to the northwest. Data obtained from 67 measured outcrops (many of which providing only a minimum thickness due to partial erosion) do not precisely define the overall areal thickness and grain-size decay (Fig. 4E). Nevertheless, the data point toward the SW bay of the lake as a likely vent site from where tephra dispersal was initially directed toward the WNW. Then, more distally, the distribution fan turns SW where we found distal ash in marine cores 120 km from the vent (Kutterolf et al., 2007). Despite of its origin we have opted to keep the name “Apoyeque Tephra” coined in earlier studies in order to avoid further confusion. The volume of the UAq is 2.2 km<sup>3</sup>, which corresponds to  $0.7 \times 10^{12}$  kg of magma (Fig. 5). Based on the downwind and crosswind ranges of the ML isopleths, eruption column heights between 25 and 31 km (Figs. 7 and 8) were estimated at wind speeds of 15 to 20 m/s. Corresponding mass discharge rates of  $3 \times 10^7$  to  $3 \times 10^8$  kg/s (Fig. 6) allow to estimate the minimum eruption duration of 12 h.

The UAq pumice bulk-rock composition is nearly identical to that of the LAq but matrix-glass compositions differ slightly by higher CaO and lower alkali contents (Figs. 9A,D and 10B,E). In addition, the UAq pumice contains a high amount of hbl phenocrysts together with predominant pl as well as opx and cpx, ti-mt, and ap (Table 2).

### 5.3. Xiloá Tephra (XT)

The Xiloá Tephra overlies massive weathered reworked tuffs with incipient paleosol formation that covers UAq (Fig. 3). Carbonized tree logs from an XT outcrop near Laguna Xiloá yielded a <sup>14</sup>C age of 6105 ± 30 years BP (Table 1). This age is slightly younger than the age of 6590 years BP reported by Bice (1985). Laguna Xiloá is the vent site of the XT but outcrops at the SW shore show that it also hosts the vent of an earlier, basaltic phreatomagmatic eruption. Moreover, the lake basin may also have been the vent site of the Los Cedros eruption (see below). Proximal outcrops of XT never show the complete succession and are dominated by alternating coarser, and fine-grained antidune structures produced by pyroclastic surges in which the white, highly vesicular pumice lapilli are well rounded.

Combined evidence from several outcrops shows that the tephra consists of a lower and an upper surge package that bracket a central, up to 150 cm thick bed of moderately sorted, weakly stratified fallout of angular to edge-rounded pumice lapilli. The lower white surge package is very fine-grained and contains lenses of ash-coated pumice lapilli. The upper surge package is more variable in grain size, contains hydrothermally altered orange-colored lithic fragments, and dunes are covered by fine-ash layers rich in accretionary lapilli. As a note of caution it should be mentioned that many outcrops in the vicinity of Laguna Xiloá display the olivine-bearing Chiltepe Tephra (see below). Bice (1985) apparently used such samples to chemically correlate the deposit he called Jiloá Pumice with outcrops at Laguna Xiloá. His Jiloá Pumice at Managua thus is actually the Chiltepe Tephra (Fig. 2).

In the more distal sections, the XT shows more clearly the tri-partite character with two white ash layers, (XA at base and XC on top) bracketing a central pumice lapilli layer XB (Fig. S2). We interpret XA and XC as distal surge deposits related to the proximally exposed antidune packages. Unit XB is a fallout deposit but only moderately sorted due to the abundance of ash. This may have resulted from mixing of pumice lapilli from the eruption column with ash from surge-related ash clouds. Although the pumice is highly vesicular and the abundance of lithics in the tephra is not unusually high, we use the abundance of ash and the dominant production of surges to infer a phreatomagmatic origin of the XT. Based on the tephra dispersal characteristics, it could be called a phreato-subplinian eruption. The isopach and isopleth maps (Fig. 4H) support a vent in the Laguna Xiloá from where the tephra was dispersed towards the WSW. Impact directions of ballistic blocks at the base of XC also point toward a vent inside Xiloá Maar. The level of Lake Managua was 9 m higher than today at the time of the Xiloá eruption (Cowan et al., 2002), such that the vent opened under water to produce a phreatomagmatic eruption. The XT volume of 1.9 km<sup>3</sup> corresponds to  $0.9 \times 10^{12}$  kg erupted magma (Fig. 5). The estimated eruption column height reached between 24 and 28 km (Figs. 7 and 8) at wind speeds of 15 to 20 m/s. The discharge rate was  $5 \times 10^7$  to  $1 \times 10^8$  kg/s (Fig. 6) which yields a minimum eruption duration of 8 h.

The XT pumice is dacitic (64–65 wt.% SiO<sub>2</sub>) with high alkali concentrations (2.1 wt.% K<sub>2</sub>O, 4.3 wt.% Na<sub>2</sub>O) as well as a relatively high (150 ppm) Zr content (Fig. 9A,C,D). The matrix-glass composition is less evolved compared to the other dacitic tephtras (Fig. 10A, B,E). The phenocryst assemblage comprises pl, opx, cpx, ti-mt, and ap.

Table 2  
Summary of tephra characteristics; abbreviations like in the heading of each tephra in the text

Unit	Age (yr BP)	Source	Composition	Sorting	Erupted mass (10 <sup>12</sup> kg)	Main eruption style	Eruption column height (km)	Color of pumice clasts	Phenocrysts content [type]	Bulk density (kg/m <sup>3</sup> )	Porosity (%)
UT	>30 ka	Unknown	Dacite	Moderate–well	–	Plinian	–	Yellowish-white	15% scattered + cluster [pl; cpx-(opx); ol xenocrysts]	400	84
FT	~30 ka	North west of Masaya	Basaltic andesite	Base = well; medium and top = moderate and poor	1.4	Plinian	24–30	Black to dark gray; dark gray red	<1% scattered [pl-(cpx)- (ol)]	720–810	67–73
LAT	23,890± 240	Apoyo Caldera	Dacite, admixed andesite	Well	1.6	Plinian to phreatomagmatic	28–34	Base white; upward increase in pink, gray and mixed	10%, cluster and scattered; [pl; cpx-opx; (hbl), ol xenocrysts]	460–570	73–79
UAT	24,650± 120	Apoyo Caldera	Dacite	UAT-1=well, UAT-2=moderate; UAT-3=moderate to well	4.7	Plinian and ignimbrite	32–35	UAT-1=white, UAT-2=white to pinkish, UAT-3=pink to pale gray	20% decreasing upward, mainly cluster, but UAT-1 also scattered large crystals [pl; cpx-opx; (hbl)]	440 fallout; 500 surges	80
LAq	~15 ka	Apoyeque (Chiltepe volcanic complex)	Rhyodacite	Moderate	0.5	(Sub) Plinian	20–23	Yellowish-white	20–30%, scattered + few cluster [hbl, pl, cpx-(opx)]	520	77
UAq	12,400± 100	Between Chiltepe and Managua	Rhyodacite	Moderate to well	1.0	Plinian	25–31	White	2%, mainly scattered only few cluster; [pl-hbl-cpx- (opx)]	430–550	78–83
XT	6105± 30	Xiloá Maar (Chiltepe volcanic complex)	Dacite	Moderate to well	0.9	Phreato-plinian	24–28	White, ash coated; increasing pink in upper part	2–5%, scattered + few cluster [pl-cpx-opx-(hbl)]	560 fallout; 610 surges	76
SAT	<6 ka	Masaya Caldera	Basalt	Well	1.2	Plinian to phreatomagmatic	24–28	Black and reddish	2% scattered [pl-cpx-(ol)]	750	50–60
MaT	3–6 ka	Chiltepe volcanic complex	Andesite to dacite	Very well	0.3	Subplinian to phreatomagmatic	10–16	Gray, red–brown to black (zoned deposit)	3–5% decreasing upward dacite: [pl-cpx-opx] andesite: pl-cpx-opx-(ol) <2% [pl-hbl-cpx-(opx)]	650 to 750	60–75
CcD	2–4 ka	Chiltepe volcanic complex	Dacite	Moderate	?	(Sub) Plinian	?	White–yellowish	<2% [pl-hbl-cpx-(opx)]	510	77
LCT	= MTL	Masaya Caldera	Basalt	Well	0.2	Plinian	18–26	Black	<2% [pl-ol-(cpx)]	700	65
MTL	2120± 120	Masaya Caldera	Basalt	Well	0.4	Plinian	22–29	black	<5%; [pl-cpx-ol; px increase to top]	700	65
CT	<2 ka	Apoyeque (Chiltepe volcanic complex)	Dacite, admixed basalt	Moderate to well	2	Plinian to phreatic	35–40	White and pink minor gray and mixed	15–25% (white = scattered; pink = cluster) [pl-cpx- opx-(hbl)]	460 (top)– 530 (base)	77–80

MT	<2 ka	Masaya Caldera	Basaltic andesite	Poor	3.9	Violent Surtseyan	–	Dark gray	5–10%; [pl–cpx–ol]		
TIL	<2120	Masaya Caldera	Basaltic andesite	Well	0.1	Subplinian	15–26	Black	<5%; [pl–cpx–ol]	700	60–70

Unit	Bed structures	Rounding/form	Bubble form/size	Lithics (%)	Lithic types
UT	Massive fallout; slightly reverse	Subangular	Moderate vesicular, large and small, elongated	<5%	Basalt, andesite; some hydrothermally altered
FT	Massive and stratified fallout, surges	Subangular to subrounded	Base = very high vesicular, rest = moderate to low, medium size, spherical	0 to 5%	Pumice clasts, basalt; some hydrothermally altered
LAT	Massive plinian to bedded Fallout, phreatom. beds at top; weakly reverse	Subangular	High vesicular; large, elongated	Lower part <5%; upper part c. 10%	Basalt, dacite, upward hydrothermally altered
UAT	Massive and stratified fallout, ignimbrite, surges; normally graded	Apoyo1 = angular to subangular (twisted to fibrous deformed); Apoyo2 = subangular; Apoyo3 = subangular to subrounded	High vesicular; Apoyo1 = tubular and medium size, Apoyo2 = elongated and medium size, Apoyo3 = spherical; large	UAT-1 = <5% (15–20% at top), UAT-2 = 10–15%, UAT-3 = 5–10%	Basalt and dacites, UAT-2 hydrothermally altered
LAq	Massive fallout, reversely graded	Subangular	High vesicular, small spherical + slightly elongated and few large elongated and deformed	10–15%	Basalt, some hydrothermally altered
UAq	Massive fallout, reversely graded	Angular to subangular	High vesicular increasing toward top, large elongated and smaller spherical,	5–10%, increasing to top	Basalt + andesite, fresh and hydrothermally altered
XT	Surges and crudely bedded fallout; normally graded	Subangular (fall) to subrounded (surge)	Moderate to high vesicular, medium to large elongated and deformed	Base: 20%; increasing to top up to 50%	Fresh basalts and dacite at base, hydrothermally altered at top
SAT	Massive and stratified fallout, surges	Subangular, fluidal shaped	Highly to moderate vesicular, medium sized, spherical and some elongated	<2%	Basalt, some hydrothermally altered
MaT	Massive fallout crudely bedded in lower part	Subangular	Medium vesicular, small (gray) and large spherical bubbles (red-brown), highly vesicular black	10–15%, decreasing to top	Basalt, dacite (obsidian), few hydrothermally altered
CcD	Massive fallout, reversely graded in total	Subangular	High vesicular, small spherical and elongated bubbles	20–35%	Basalt + andesite, some hydrothermally altered
LCT	Stratified fallout, surge beds	Subangular, fluidal shaped	High to moderate vesicular, medium to large sized, spherical and some elongated	<5%	Basalt, fresh and hydrothermally altered
MTL	Stratified fallout and surge beds, mid acc. Lap. layer, uppermost reversely graded	Subangular, fluidal shaped	High to moderate vesicular ridicule like, medium size, mainly spherical	<1%, upper most up to 3%	Basalt, fresh and hydrothermally altered
CT	Reversely-graded fallout	Angular to subangular	White = moderate to high vesicular, small and medium sized elongated bubbles; pink = high vesicular, large spherical bubbles in cluster; gray = low vesicular, fine spherical bubbles	50% (basal), 20% (middle), 10% (top)	Basalt, fresh and hydrothermally altered, dacite
MT	Surge beds			70–90%	Basalt, gabbro
TIL	Massive fallout	Subangular, cauliflower	Moderate vesicular, medium size, spherical	1–5%	Basalt, some hydrothermally altered

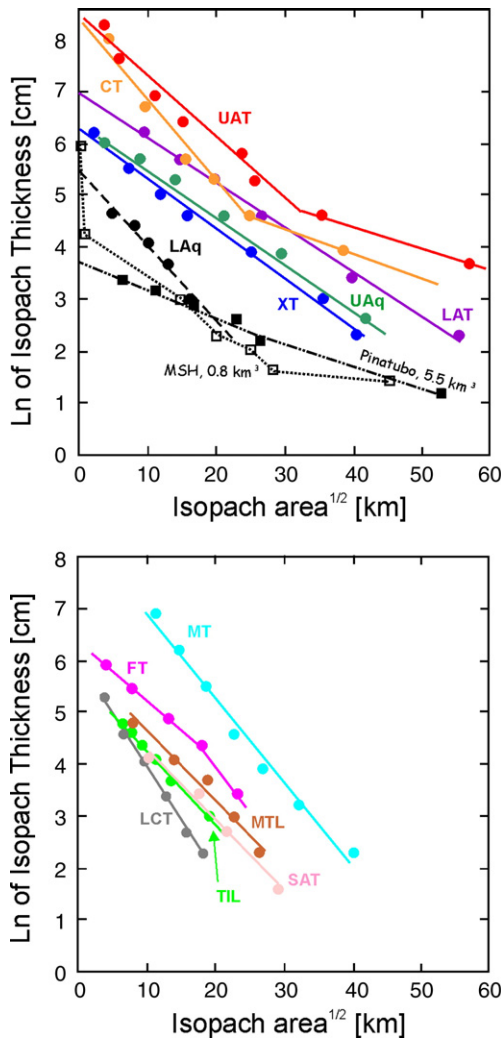


Fig. 5. Ln (isopach thickness) versus square-root (isopach area) diagram for all tephra. Linear regressions as indicated were used to calculate tephra volumes after Fierstein and Nathenson (1992). Data for the mafic tephra are from Pérez and Freundt (2006) and Wehrmann et al. (2006). Date from Pinatubo 1991 and Mt. St. Helens 1980 (MSH) are shown for comparison and are from Houghton et al. (2000) and Paladio-Melosantos et al. (1996). Abbreviations as in Fig. 3.

5.4. Mateare Tephra (MaT)

The newly identified Mateare Tephra is only exposed along the shore of Lake Managua northwest of the town of Mateare and in the lowlands south to southeast of this town. It usually rests on sandy sediments that cover an erosional unconformity (U2 in Fig. 2) cutting variably deep into the underlying XT (Fig. 3). The MaT and the underlying sand were discussed by Freundt et al. (2006b) and a brief summary shall suffice here. The most prominent feature of the MaT is its compositional zonation that ranges from dacitic at the base to andesitic at the top. The tephra can be

divided into four units. Basal unit A is a stratified fallout of high-silica dacite pumice that represents an initial unsteady phase of the eruption influenced by external water. The Mateare sand layer lies on top unit A in some outcrops and is interpreted to be the product of syn-eruptive tsunamis in Lake Managua that eroded unit A in most outcrops. Overlying unit B is a massive, well-sorted fallout deposit of pale gray and pinkish dacitic pumice *c.* 2 m thick. A rapid change in composition at the top leads to the ~20-cm-thick fallout unit C composed of black andesitic pumice lapilli. Units B and C together are the product of a fairly steady plinian eruption that was little affected by the change in magma composition. The topmost unit D is a stratified tuff

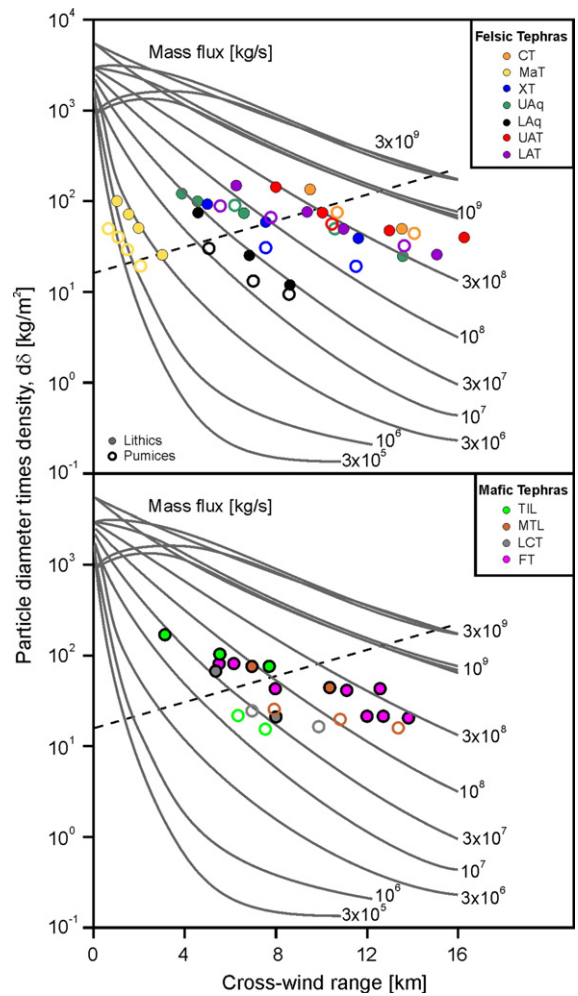


Fig. 6. MP and ML clast size × density versus isopleth cross-wind range of the tephra compared to model results of Wilson and Walker (1987). Includes data from Freundt et al. (2006b), Pérez and Freundt (2006), and Wehrmann et al. (2006). Note that model results below the dashed line are less reliable since Wilson and Walker used a top-hat velocity profile that did not capture lateral velocities in the higher part of the eruption column.

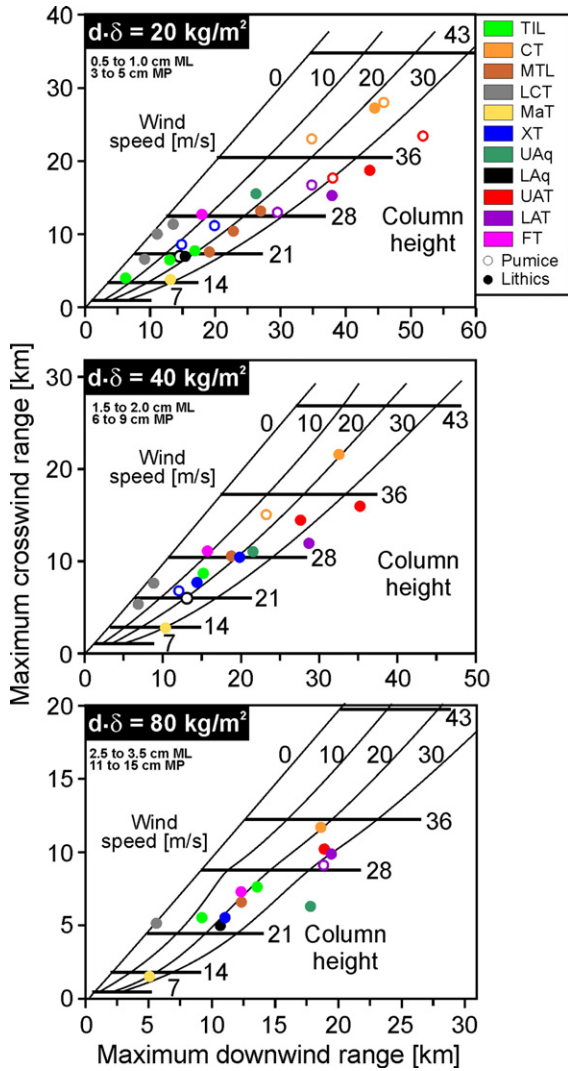


Fig. 7. Diagrams of crosswind range versus downwind range for ML and MP isopleth data compared to model results of Carey and Sparks (1986). Clasts were selected to be close to, but are not identical to, the diameter  $\times$  density products shown. The range of pumice and lithic sizes are given in diagrams and we used densities given in Table 2. Horizontal grid lines indicate eruption column heights (in km) and diagonal grid lines show wind velocities (in m/s). Data from Freundt et al. (2006b), Pérez and Freundt (2006), and Wehmann et al. (2006) are also included.

rich in accretionary lapilli that represents a terminal phreatomagmatic phase of the eruption.

Because all available outcrops lie on an almost straight line, the isopach and isopleth patterns are poorly constrained. The distribution data do, however, point to a fallout dispersal toward the WNW from a vent in the lowland east of Mateare that is now buried (Fig. 4 in Freundt et al., 2006b). A conservative estimate of the erupted tephra volume yields  $\sim 1 \text{ km}^3$ , which corresponds to  $0.5 \times 10^{12} \text{ kg}$  of magma of which 90% is

dacitic (Fig. 5). The estimated column height was 12 to 16 km (Figs. 7 and 8) which corresponds to a magma discharge rate of 1 to  $3 \times 10^6 \text{ kg/s}$  (Fig. 6) and to a minimum eruption duration of several hours.

The MaT differs compositionally from all other tephras considered in this study by its strong compositional zonation and by the elemental concentrations in its dacitic component, which is poor in  $\text{K}_2\text{O}$  and rich in Sr (Figs. 9A, C, D and 10C, D, E). Phenocrysts include pl, opx and lesser cpx.

Northwest of Mateare, the MaT is partly eroded (U3 in Fig. 2) and overlain by several-meter thick fluvial channel fills of reworked tephra. The abundance of channels suggests that an active drainage system developed after the Mateare eruption. However, overlying weathered massive tuffs with a paleosol on top underneath the Chiltepe Tephra, indicates that this flooding terminated well before the Chiltepe eruption.

### 5.5. Los Cedros Tephra (CdT)

Los Cedros Tephra is also a newly identified pumice fallout deposit that occurs between Mateare and western Managua. Southeast of Mateare, CdT overlies MaT unit D tuff that is strongly weathered to a depth of 15 cm. Here,

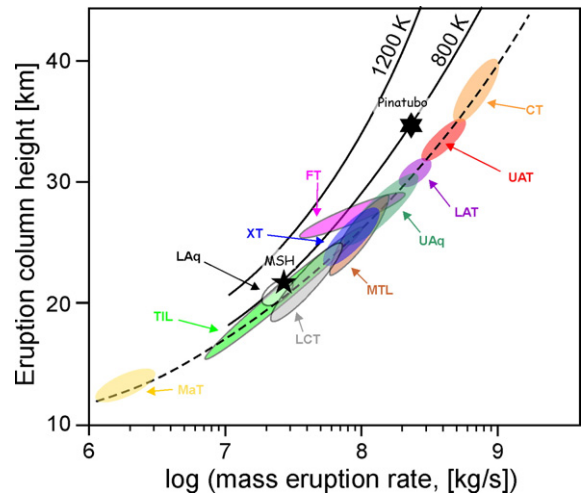


Fig. 8. Diagram of logarithm of mass eruption rate versus eruption column height in which the ellipses show the range of data for each tephra estimated from Figs. 6 and 7. Black curves show modeled variation for temperatures of 800 K and 1200 K after Woods (1988). The Nicaraguan tephras lie on a separate dashed curve, which represents an artifact of combining the results of two different modeling approaches after Wilson and Walker (1987, magma discharge rate) and Carey and Sparks (1986, eruption column heights) in one diagram to test reliability of the estimated Nicaraguan eruption column heights. Stars indicate data for Pinatubo 1991 and Mt. St. Helens 1980 (MSH) eruptions from Houghton et al. (2000) and Paladio-Melosantos et al. (1996) for comparison.

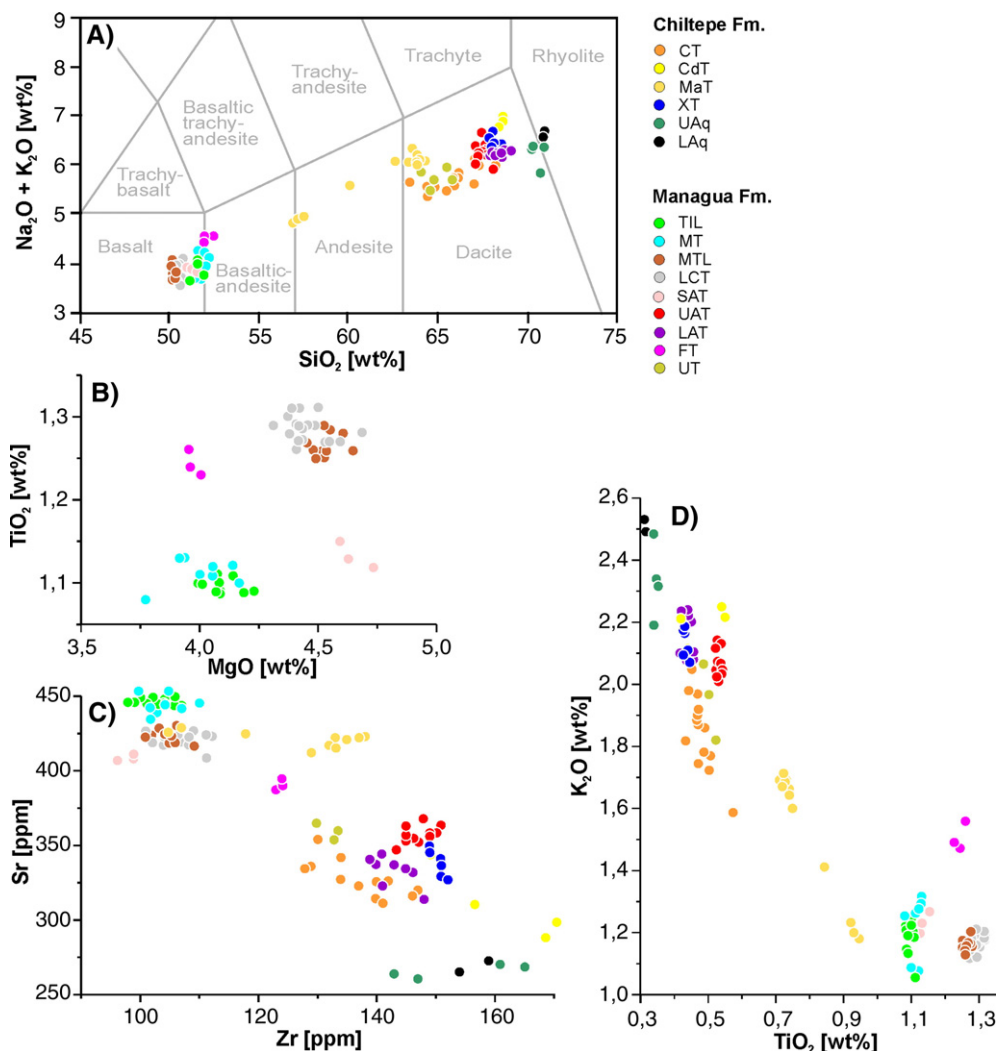


Fig. 9. Selected bulk-rock chemical variation diagrams (data normalized to anhydrous compositions) showing the compositional differences between the juvenile components of the tephra. 2-sigma analytical precision is better than 1% for major, <5% for minor and 5–8% for trace elements. A) TAS diagram showing a compositional range from basaltic to rhyodacitic compositions. B) The  $\text{TiO}_2$  versus  $\text{MgO}$  diagram is particularly useful for distinguishing the mafic tephra. Discrimination of all tephra is possible in (C) the Sr versus Zr and (D) the  $\text{K}_2\text{O}$  versus  $\text{TiO}_2$  diagrams.

CdT forms a single inversely graded fine-to-medium grained pumice lapilli fallout bed ~60 cm thick that is eroded at the top. In western Managua, CdT is sandwiched between basaltic hydroclastic deposits of Nejapa–Miraflores volcanism and overlies some 40 cm of yellow weathered tuffs. Here, the inversely graded main part of the CdT is ~40 cm thick and is overlain by a second finer-grained pumice lapilli layer whose contents of lithic fragments and ash increase upwards.

Thickness and grain-size relations between the 10 outcrops of the CdT that we have found so far suggest a source at the Chiltepe peninsula and a dispersal axis toward the SSW. We suspect that the vent lies within Laguna Xiloá where CdT reaches maximum observed

thickness of >1.5 m. A preliminary estimate of the tephra volume yields ~0.5 km<sup>3</sup>.

The bulk composition of the dacitic CdT is similar to the XT, and its glass composition is best characterized by its high iron and medium calcium contents as well as the highest zirconium concentrations in this area (Figs. 9C and 10A). In contrast to the white XT pumice, the CdT pumice ranges in color from white to pink and light gray and contains phenocrysts of hbl and grass-green opx.

### 5.6. Chiltepe Tephra (CT)

We also newly identified the dacitic Chiltepe Tephra, which was produced by the youngest and biggest plinian

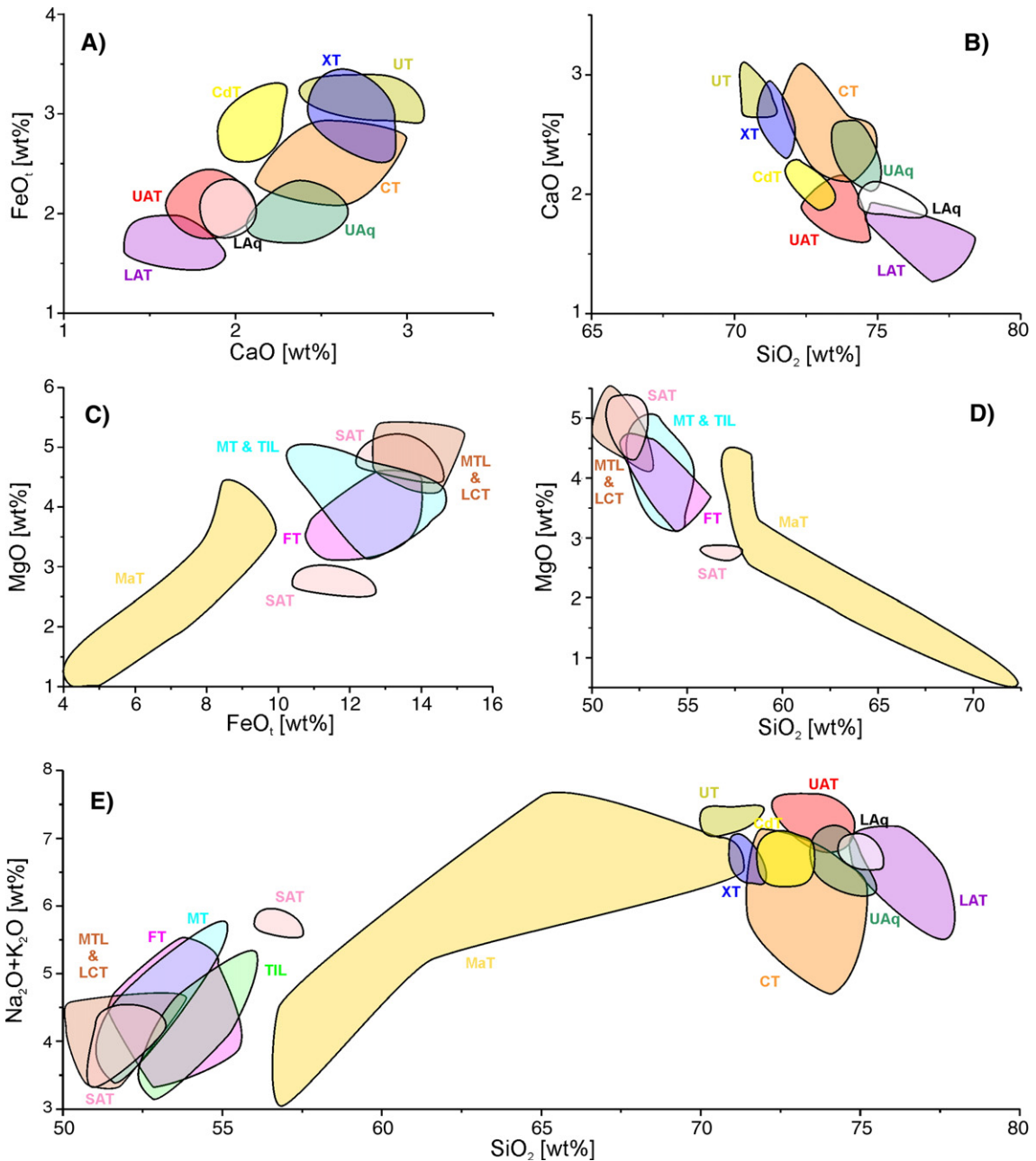


Fig. 10. Matrix-glass compositions of pumice and scoria lapilli of the tephra (data normalized to anhydrous compositions). 1-sigma analytical precision is better than 2% for the elements shown. Each tephra field comprises 20–30 spot analyses of 1–5 sample lapilli from outcrops where stratigraphic relations were unambiguous. Felsic tephra glass compositions are reasonably distinct and combining diagrams A, B, E proved most useful to substantiate stratigraphic correlations. Mafic tephra glasses are less distinct but combining diagrams C, D, E can support correlations. Note that SAT glasses occupy two distinct fields of composition as discussed in the text. The wide fields of MaT reflect the strong compositional zonation of this tephra.

eruption from the Chiltepe volcanic complex (Fig. 3). The widespread CT, however, erupted from the Apoyeque crater as demonstrated by our isopach and isopleth maps as well as by ~80 m thick proximal deposits at the crater rim. In western Managua, CT overlies the Masaya Triple

Layer dated at  $2120 \pm 120$  years BP (Pérez and Freundt, 2006) and is overlain by the Masaya Tuff. The Chiltepe eruption is thus younger than 2100 years.

The proximal tephra section reveals a complex eruption history, discussed elsewhere. The eruption

initiated with a phreatomagmatic phase that produced a thick white ash, as well as plinian fallouts including horizons rich in ballistic lava blocks. Towards the top, the fallout deposits become increasingly interrupted by surge deposits. The surges left the crater through the low southern notch sweeping across Laguna Xiloá toward Managua. At the end of the multiple plinian phase, a thick ash-rich lava-block breccia was emplaced by a phreatomagmatic event clearing the crater. A phreatic terminal phase of the eruption formed a 20-m-thick tuff-ring around the crater. Outside the southern surge fan, medial to distal sections of CT only contain plinian fallout layers and a poorly preserved phreatomagmatic white ash at the top. The pumice lapilli fallout is overall inversely graded and consists of a lower stratified part, a massive to crudely stratified middle part, and a massive upper part (Fig. S3).

The thickness and grain-size dispersal patterns of the CT were deduced from 58 outcrops (Fig. 4G) and show a change from a west-directed fan axis at proximal locations to an SW direction in distal areas where a 3 to 14 cm thick ash layer is preserved in marine sediments 350 km from source (Kutterolf et al., submitted for publication-b). The on-shore volume of the CT is  $4 \text{ km}^3$  which corresponds to  $2 \times 10^{12} \text{ kg}$  of magma (Fig. 5). The eruption column height is estimated at 35 to 40 km (Figs. 7 and 8) at wind speeds of  $\sim 20 \text{ m/s}$ . The discharge rate was  $5 \times 10^8$  to  $8 \times 10^8 \text{ kg/s}$  (Fig. 6) and the minimum duration of the plinian phase of the eruption might have been 6 h.

The dacitic white and highly vesicular pumice of the CT is more crystal-rich compared than the other Chiltepe Formation tephra. Phenocrysts comprise pl, opx, cpx, ti-mt, and ap; minor hbl is observed in thin section. Olivine crystals up to 1 cm in size, with occasional dark rims of mafic melt, are characteristic of CT pumices. The CT pumice bulk-rock composition is distinctively low in  $\text{K}_2\text{O}$  and Zr while its glass composition is intermediate between that of XT and UAq pumices (Figs. 9C,D and 10A,B,E).

## 6. The Las Sierras Formation

We have so far only studied the two tephra layers that form the top of the Las Sierras Formation in the Managua–Masaya area: the basaltic–andesitic Fontana Tephra and the dacitic Unicit Tephra (Fig. 2). A more detailed investigation of the Las Sierras Formation still has to be done.

### 6.1. Unicit Tephra (UT)

The Unicit Tephra is a 20 to 65 cm thick massive pumice lapilli bed that is slightly inversely graded at the base and changes to normally graded with a higher

content of ash at the top. The few available outcrops indicate a southerly decrease in thickness and grain size but are insufficient to construct isopach and isopleth maps. The most northerly site of 65 cm maximum thickness and  $\text{MP}=8 \text{ cm}$ ,  $\text{ML}=2 \text{ cm}$ , might be only a few kilometers from its vent position, possibly within southern Lake Managua. The UT volume was crudely estimated by comparison with other deposits at  $c. 1 \text{ km}^3$ .

The pumice is dacitic (64–65 wt.%  $\text{SiO}_2$ ; Fig. 9A). Its best distinguishing feature is its least evolved glass composition in comparison to other pumice glasses, and its high iron content (Fig. 10A,E). Phenocrysts comprise pl, opx, cpx, ti-mt and minor ol.

The age of the UT is unknown but we estimate it to be  $>60 \text{ ka}$ . The UT is overlain by locally variable sediments such as lahar, debris flow, and other epiclastic deposits, as well as tuff beds containing abundant accretionary lapilli representing local mafic phreatomagmatic eruptions that occurred during the intervening time between the Unicit and Fontana Tephra.

### 6.2. Fontana Tephra (FT)

The overlying basaltic–andesitic Fontana Tephra, is equivalent to the Fontana Lapilli of Williams (1983a) and to the Masaya Lapilli Bed of Bice (1985). Wehrmann et al. (2006) discussed this deposit in more detail. The FT is a layered sequence of black, highly vesicular scoria lapilli fallout beds that have a wide, plinian dispersal toward the NW of Masaya Caldera. Wehrmann et al. (2006) argue that the most likely vent position was some kilometers to the west outside the Masaya Caldera. The erupted tephra volume amounts to  $1.4\text{--}1.8 \text{ km}^3$  (Fig. 5), equivalent to  $1.1\text{--}1.4 \times 10^{12} \text{ kg}$  of magma. Maximum eruption column heights were estimated between 24 and 30 km with a mass discharge rate of  $1.3$  to  $2.6 \times 10^8 \text{ kg/s}$  (Figs. 7 and 8). We interpret mafic ashes between 55 and 68 ka in marine sediment cores from cruises M54/2, M66/3a and SO173/3 offshore Nicaragua as distal deposits of FT (Kutterolf et al., submitted for publication-b; Kutterolf et al., 2007). This implies a significantly larger bulk volume as well as a distal dispersal toward the WSW.

The Fontana basaltic andesite (52–53 wt.%  $\text{SiO}_2$ ) differs from mafic tephra of the Managua Formation by its high  $\text{TiO}_2$ ,  $\text{K}_2\text{O}$  and Zr concentrations at relatively low MgO bulk-rock concentrations. Glass chemistry also shows highest alkali and lowest MgO and FeO concentrations, which facilitates its distinction from other tephra (Figs. 9B,C,D and 10). The occurrence of rare phenocrysts of pl, cpx, and ol is not distinctive.

## 7. The Managua Formation

The Managua Formation comprises seven tephra units (Fig. 2 and 3) emplaced during the past 25 ka that have compositions from basalt to rhyolite differing from the predominately dacitic tephtras of the Chiltepe volcanic complex. These tephtras formed by highly explosive eruptions from vents at the Apoyo and Masaya calderas.

### 7.1. Lower Apoyo Tephra (LAT)

Sussman (1985) inferred that the Apoyo caldera subsided during two paroxysmal eruptions separated from each other by a period of quiescence. His first eruption comprises the white pumice fallout layer A, the Apoyo ignimbrite, and a phreatomagmatic tuff layer B, whereas pumice fallout layer C above a paleosol represents a second eruption. All these units are composed of pumice of identical dacitic composition. Although we also recognized two separate Apoyo eruptions, our work has led to different conclusions regarding the stratigraphic relationships. We have identified the LAT composed of characteristic pumice with ol-xenocrysts that is compositionally distinct from the Upper Apoyo Tephra (UAT), which includes the Apoyo ignimbrite (Figs. 3 and 9 and S4). The LAT and UAT are separated by a paleosol and an erosional unconformity. Hence, the break in activity occurred before and not after, the ignimbrite formation, and therefore also prior to major caldera collapse. The Apoyo Pumice of Bice (1985) corresponds to our UAT while his Lower Apoyeque Pumice is our LAT (Fig. 2) as substantiated by chemical compositions.

The age of the LAT is constrained by a  $^{14}\text{C}$  age of  $23,890 \pm 240$  years BP obtained on the immediately underlying paleosol (Table 1). The pumice fallout deposit is weakly reversely graded and faint bedding can be recognized in the upper third portion. In proximal sections the pumice layer is overlain by an up to 4 m thick stratified sequence of lithic-rich lapilli and ash beds. Most of these beds are fallout from terminal phreatomagmatic to phreatic eruptions; some ash beds with low-angle cross bedding represent episodic pyroclastic surges (Fig. S4). The topmost deposit is a finely stratified tuff with accretionary lapilli at the west rim and a wavy bedded surge ash at the southeastern rim of the caldera. The entire phreatomagmatic sequence thins rapidly with distance and grades into a normally graded yellow–pink lithic-rich ash layer at the top of the pumice fallout in medial exposures.

Isopach and isopleth maps for the LAT are based on measurements taken at 53 outcrops around the Apoyo

Caldera (Fig. 4C). Isopach and isopleth axes are oriented toward the NNW in proximal areas and turn toward the NW in the medial range reflecting an unusual vertical wind profile as discussed below. Based on data down to the 10-cm isopach (Fig. 5) a minimum volume of LAT is estimated at  $2.9 \text{ km}^3$ , which corresponds to  $1.6 \times 10^{12}$  kg of magma mass. The estimated eruption-column height was 28 to 34 km at wind speeds of 15 to 20 m/s (Figs. 7 and 8), which corresponds to a mass discharge rate of  $0.3\text{--}3 \times 10^8$  kg/s (Fig. 6) and yields minimum eruption duration of 3 h.

The bulk-rock composition of the pumice clasts is dacitic with high silica (67.9–69.0 wt.%) and moderate to high alkali contents (2.1 wt.%  $\text{K}_2\text{O}$ , 4.1 wt.%  $\text{Na}_2\text{O}$ ) (Fig. 9A). The LAT can be discriminated from the UAT by lower  $\text{TiO}_2$  and Sr bulk-rock concentrations as well as by distinct matrix-glass compositions (Figs. 9C,D and 10A,B,E). The mineral assemblage comprises phenocrysts of pl, opx, cpx, minor ti-mt and ap as well as ol-xenocrysts.

### 7.2. Upper Apoyo Tephra (UAT)

Charcoal collected from the lower part of the UAT yielded a radiocarbon age of  $24,650 \pm 120$  years BP (Table 1); Sussman (1985) reports a radiocarbon age of  $22,800 \pm 1000$  years BP for charcoal in the ignimbrite. Both dates overlap with the LAT date suggesting a break in time of only a few hundred years between the LAT and UAT eruptions. In proximal exposures, the Lower and Upper Apoyo tephtras are separated by a weathering horizon and local unconformity or paleosol on top of the uppermost LAT phreatomagmatic tuff (Fig. 3).

Near the caldera the UAT can be divided into three distinct packages. UAT-1 is a moderately to well-sorted stratified white pumice lapilli fall deposit interrupted by several thin ash beds. It represents the first, slightly unsteady plinian phase of the eruption. The following UAT-2 succession consists of surge, fall, and pyroclastic flow deposits. About halfway through this interval, several lithic-rich surge and fallout layers contain abundant hydrothermally altered lithics. Distinct pink ash beds consist entirely of finely comminuted hydrothermally altered material. The eruption phase that produced UAT-2 was highly unsteady; frequently collapsing eruption columns deposited thin fallout beds alternating with surge and flow deposits. An unstable vent and tapping of the hydrothermal system favored magma–water interactions that culminated with the phreatic eruption of an entirely lithic surge bed. Pyroclastic flows and surges locally carved deep erosion channels into underlying deposits. The pyroclastic flows mainly flowed to the east

and south to form the thick ignimbrite succession between Apoyo and Mombacho and around Granada as described by Sussman (1985). Several pyroclastic flows also surmounted the higher western caldera rim to pond in the valley of San Juan del Oriente; in outcrops at the western caldera wall, however, these flows only left thin veneers of red–brown ash, some of which cover erosional unconformities. UAT-2 is locally eroded and replaced by reworked sediment suggesting a hiatus in eruption before formation of the third package UAT-3, that is distinguished by its large (up to 25 cm) pink pumice clasts. UAT-3 is composed of very coarse-grained surge and fallout layers. Most of these are poor in lithics. At the northern caldera rim, however, a basal surge unit is rich in lava blocks. The overlying ~20-m-thick pumice block-fallout contains only few intercalated surge-ash horizons although a thick surge succession is found outside the caldera. At the western rim, surge deposits with abundant pink pumice-blocks dominate the entire UAT-3 succession. In between, at the northwestern rim, UAT-3 appears as a pink pumice block-fall with a low-angle lensoid structure, suggesting that fallout emplacement was influenced by simultaneously passing surges. UAT-3 corresponds to the coarsest beds in the more distal sections and thus represents the most powerful plinian phase of the eruption. Nevertheless, we interpret that the eruption column frequently became unstable and suffered partial collapse that shed pyroclastic surges into different directions.

In medial to distal sections outside the area of ignimbrite distribution and beyond the rapidly thinning, radially distributed surge deposits, the UAT has also a tripartite structure (Fig. 3; S5). A lower white pumice layer represents UAT-1. A central layer in which white lapilli and pink ash beds alternate, corresponds to UAT-2. The coarsest, pink top layer is unit UAT-3 fallout. The cumulative thickness and grain-size dispersal patterns of the UAT, were obtained by measuring 58 outcrops (Fig. 4B). They display a change in direction from a medially WNW directed fan axis to an SW direction in distal areas where a 7 to 18 cm thick ash layer is preserved 400 km from source in marine sediments (Kutterolf et al., submitted for publication-b). The on land tephra volume derived from the isopach map is calculated at  $7.5 \text{ km}^3$  (Fig. 5). Adding the volume of  $8.5 \text{ km}^3$  of the ignimbrite (Sussman, 1985) results in a total volume of  $16 \text{ km}^3$  for the UAT without the distal part. The minimum erupted magma mass then is  $4.7 \times 10^{12} \text{ kg}$ . The eruption-column height is estimated at 32 to 35 km (Figs. 7 and 8) at wind speeds of 30 m/s. Discharge rates of 3 to  $7 \times 10^8 \text{ kg/s}$  (Fig. 6) suggest a minimum eruption duration of 15 h. However, the eruption was frequently interrupted and may have lasted several days or weeks.

The Upper Apoyo pumice is a dacite with high silica (67–68 wt.%) and moderate to high alkali concentrations (2.1 wt.%  $\text{K}_2\text{O}$ , 4.1 wt.%  $\text{Na}_2\text{O}$ ) (Fig. 9A). High  $\text{TiO}_2$  and Sr bulk-rock and very high alkali concentrations in glass facilitate its distinction from other tephtras (Figs. 9C,D and 10E). The phenocryst assemblage comprises pl, opx, cpx plus minor ti-mt and ap.

### 7.3. San Antonio Tephra (SAT)

South of Managua, the medial UAT is overlain by the UAq and a white ash layer that chemically correlates with the XT; all three are separated by yellowish altered tuffaceous sediments with paleosols. Above this sequence and another paleosol lies the San Antonio Tephra, which is therefore less than 6100 years old and was newly identified by Pérez and Freundt (2006).

The SAT is a sequence of black scoria falls overlain by surge deposits that we found northwest, north, and south of Masaya Caldera. The most proximal outcrops show a lower sequence of alternating well-sorted coarse-ash to fine-lapilli scoria fall layers and fine-grained phreatomagmatic tuffs. This is followed by a prominent well-sorted layer of vesicular fluidally-shaped black scoria lapilli (layer A6 of Pérez and Freundt, 2006) and a very distinctive lapilli layer (A7) with a high content of yellowish and pinkish hydrothermally altered lithic fragments. These two layers are markers that can be traced to distal exposures. The sequence is dominated upwards by surge deposits with cross-bedding, low-angle dune structures and intercalated accretionary lapilli-rich beds. The unit ends with a well-sorted deposit of mixed vesicular and dense reddish lapilli.

A reconstruction of the thickness distribution of the SAT is limited by the few available outcrops and variable post-emplacement erosion. The isopach map for the most widespread layer A6 (Fig. 11A in Pérez and Freundt, 2006) shows that the eruption took place in Masaya Caldera with a tephra dispersal toward the NW. The volume of layer A6 has been estimated at  $0.7 \text{ km}^3$ , which corresponds to  $1.2 \times 10^{12} \text{ kg}$  magma (Pérez and Freundt, 2006; Fig. 5), and provides a minimum value for the SAT eruption. Calculated eruption-column height for A6 is 24 to 28 km at wind speeds of 15 to 20 m/s, with discharge rates of  $5 \times 10^7$  to  $1 \times 10^8 \text{ kg/s}$ .

The juvenile fragments of SAT consist mostly of highly vesicular sideromelane lapilli and denser tachylite. The crystal content is low (<10% vesicle-free) and represented mostly by pl and ol with rare cpx. The SAT differs by its low-Ti and high-Mg composition from the other mafic tephtras considered here (Fig. 9B,D). Glass compositions of the mafic tephtras are less distinctive. A peculiar feature

of the SAT scoria, however, is the occurrence of two distinct glass compositions (Fig. 10C,D,E). Highly vesicular scoria lapilli contain distinctly more evolved glass than moderately vesicular fragments and are restricted to layers at the base of the tephra succession.

The SAT is overlain by a reworked volcanoclastic deposit that is capped by a regional erosional unconformity (U4 in Fig. 2) similar to the Mateare region where erosional unconformities occur above the XT and above the MaT (U2, U3 in Fig. 2, respectively). We think that these regional unconformities west, south and north of Managua are time-equivalent to a period of enhanced erosion. This is why we place the SAT below the MaT in our composite section (Fig. 2) although we could not find any direct geologic evidence to support this.

#### 7.4. La Concepción Tephra (LCT)

La Concepción Tephra is exposed south of Masaya Caldera, where it reaches up to 2 m in thickness. It is locally separated from the overlying Masaya Tuff by minor erosional unconformities.

Pérez and Freundt (2006, Fig. 3) identified 16 layers (B1 through B16), comprising 8 well-sorted scoria lapilli fallout layers alternating with indurated phreatomagmatic ash layers. The well-sorted layers B1, B3, and B5 are composed of highly vesicular black lapilli to coarse-ash, with small amounts of basaltic lava lithic fragments (~1–3%). Layer B5 is the thickest lapilli bed and a useful marker in all outcrops. It is vaguely stratified by vertically alternating grain size and composed of characteristic fluidally-textured highly vesicular lapilli. Above B5, the well-sorted lapilli layers B7, B9, and B11 consist of both, highly vesicular (with a sideromelane matrix) and dense to poorly vesicular (with a tachylite matrix) scoria lapilli. The fraction of denser clasts as well as the amount of hydrothermally altered lithic fragments increases upward through the succession.

Intercalated gray, fine-grained tuff beds are mostly massive and cemented; some of them contain accretionary lapilli, armored lapilli, dispersed glassy scoria fragments and plant moulds. The uppermost tuffs (B12, B15) are thicker, poorly sorted, with low-angle cross-bedding and dune-structures and laterally changing thickness suggesting an origin by pyroclastic surges.

The isopach distribution pattern is to the south away from the Masaya Caldera but with an almost circular, low-wind isopach pattern. The estimated tephra volume of 0.2 km<sup>3</sup> corresponds to 2.0 × 10<sup>11</sup> kg of magma (Fig. 5). The estimated eruption column height is 18 to 26 km (Figs. 7 and 8) which corresponds to mass discharge rates of 3 to 7 × 10<sup>7</sup> kg/s (Fig. 6).

#### 7.5. Masaya Triple Layer (MTL)

The Masaya Triple Layer, originally described by Bice (1985) and Williams (1983a), is composed of 7 major scoria lapilli fallout beds intercalated with 4 major and several minor ash beds (Layers C1 through C10 of Pérez and Freundt, 2006, Fig. 5). The highly vesicular scoria lapilli are fluidally textured at the base but assume round shapes upward through the deposit where the lithics increase. Desiccation cracks on the surface of some ash beds indicate wet emplacement and minor breaks in deposition. Massive to laminated ash beds in medial to distal sections correspond to packages of thin lapilli and ash layers in proximal sections. Some of these tuff layers do not extend to great distances where the stratigraphic succession becomes simpler. Radiocarbon dating of plant remains in the MTL yields an age of 2120 ± 120 years BP (Pérez and Freundt, 2006; Table 1), which is much younger than the >7000 years estimate of Bice (1985) based on an erroneous stratigraphic relation with the XT.

The dispersal axis of the deposit is to the northwest from Masaya caldera and the tephra volume was estimated at 0.4 km<sup>3</sup>, which corresponds to 4.3 × 10<sup>11</sup> kg of magma (Fig. 5). The estimated eruption column height is 22 to 29 km (Figs. 7 and 8) at wind speeds of ~20 m/s, with a the mass discharge rate of 6 × 10<sup>7</sup>–1.5 × 10<sup>8</sup> kg/s (Fig. 6).

Scoriae from MTL and LCT both contain ol, pl, and cpx phenocrysts and have almost identical concentrations of both major and trace elements in the bulk rock as well as in glass, although some LCT samples extend to slightly more evolved, lower MgO compositions. They differ from other mafic tephros of the Masaya Caldera by relatively high MgO and TiO<sub>2</sub> but low Sr concentrations (Figs. 9B,C,D and 10C,D).

The MTL and the LCT both occur at the same relative stratigraphic level, both had their source vent in the western part of the caldera, and both have almost identical magmatic compositional ranges. Nonetheless, they differ by their internal lithologic architecture and regional distribution patterns. Pérez (2007) has developed a correlation model of MTL and LCT that plausibly accounts for lateral lithologic changes in individual layers and explains the MTL–LCT facies as the product of a multi-phase eruption that lasted considerable time and experienced repeated changes of wind direction and eruptive mechanisms.

#### 7.6. Masaya Tuff (MT)

The gray mafic Masaya Tuff is a phreatomagmatic surge deposit that extends to more than 35 km from its source, the Masaya Caldera (Pérez and Freundt, 2006). It was first described by Krusi and Schultz (1979),

Williams (1983a) and Bice (1985). It is separated from the underlying MTL–LCT by yellow weathered tuff layers, local erosional unconformities, and west of Managua by the intercalated CT. This suggests an age of less than 2000 years, much younger than the 3000 to 6000 years estimated by Bice (1985).

The MT is radially distributed around the Masaya caldera and is mainly composed of ash-rich antidune beds containing dense to poorly vesicular juvenile basalt lapilli and fragments of pre-existing basaltic lavas in a vitric fine ash matrix. The juvenile fragments are mostly tachylitic with pl, ol, and scarce cpx phenocrysts.

The MT cumulative thickness reaches 15 m. Pérez and Freundt (2006) defined four main units in a complete section of the MT, based on intercalated accretionary-lapilli tuffs and structural changes. A basal breccia occurs within 1 km to the NE from the caldera rim. In distal sections, the MT is a package of yellowish indurated planar laminated fine-ash benches with accretionary lapilli. The isopachs have a radial pattern around the caldera but with faster thinning to the south while the <20 cm isopachs show some elongation to the NW where the wind affected distal surge clouds. The estimated tephra volume of 3.9 km<sup>3</sup> corresponds to  $1.9 \times 10^{12}$  kg of magma (Fig. 5). The lithological characteristics of the MT support an interpretation as a pyroclastic surge deposit (Krusi and Schultz, 1979; Williams, 1983a). The surges were wet, as indicated by their fine grain size and the abundance of accretionary lapilli. They formed from phreatomagmatic eruptions that probably involved lake water filling the pre-existing caldera basin.

### 7.7. Ticuantepe Lapilli (TIL)

A well-sorted black scoria lapilli fallout deposit, the Ticuantepe Lapilli (Pérez and Freundt, 2006), immediately overlies the MT west of Masaya caldera. It consists of 4 well-sorted lapilli layers intercalated by 3 lithified ash-rich layers. Vesicular scoria lapilli occur together with dense, round juvenile lapilli and contain ~5% of pl, ol, and rare cpx phenocrysts in a tachylitic groundmass with pl and cpx microlites. The fallout is distributed toward the northwest and the tephra volume was estimated at 0.3 km<sup>3</sup> ( $1 \times 10^{11}$  kg of magma; Fig. 5) with a height of the eruption column of 15 to 26 km (Figs. 7 and 8), and a discharge rate of  $1.5 \times 10^7$  to  $1 \times 10^8$  kg/s (Fig. 6).

The MT and TIL juvenile lapilli have the same chemical composition, with some TIL samples extending to lower MgO concentrations. MT and TIL differ from the other mafic Masaya tephtras by their more evolved basaltic–andesitic compositions and a low TiO<sub>2</sub> content (Figs. 9B and 10E).

The occurrence of the TIL in direct contact to the underlying MT with no indication of a time break, the similar phenocryst assemblage (pl, ol and cpx) and the almost identical basaltic–andesitic juvenile composition of both deposits, all suggest that the TIL represents a terminal phase of the phreatomagmatic MT eruption. The high eruption column that produced the TIL fallout was probably facilitated by a decreasing influence of external water on the eruption process as indicated by the higher vesicularity of the scoria.

## 8. Conclusions

### 8.1. The next big eruption

Of the three possible candidates, Apoyo, Masaya, and Chiltepe, for the next large eruption in the area, Apoyo caldera produced the biggest eruption (UAT) yet recorded in Nicaragua. The two described ~24 ka old eruptions from Apoyo together produced at least 60 km<sup>3</sup> (Kutterolf et al., submitted for publication-b) of rhyodacitic tephra and caused the collapse of the caldera. There is no evidence for subsequent activity. Apoyo therefore appears to be a volcano with long repose times (10<sup>4</sup> years) and existing data give no indication on when or how this volcano might re-awaken although hot saline water intrusions (4000 ppm NaCl and c. 220 °C; Zúñiga et al., 2003) into the lake indicate that the Apoyo magma system might still be active.

Masaya caldera experienced three intense eruptions during the past ~6 ka with a total tephra volume of at least 7 km<sup>3</sup> demonstrable on land. Our offshore stratigraphic work suggests these tephtras combine to >25 km<sup>3</sup>, with the ~6 ka SAT alone accounting for 14 km<sup>3</sup> and the <2 ka MT for 6.6 km<sup>3</sup> (Kutterolf et al., submitted for publication-b). These two eruptions are the only ones demonstrated to have a sufficiently large volume to have formed a caldera with ~7 km<sup>3</sup> volume deficit. We believe that the SAT eruption initiated the subsidence of the Masaya caldera, with possible additional subsidence occurring during the later eruptions. The ~24 ka Apoyo tephtras occur as thick layers outside but not within the Masaya Caldera walls; we suspect they are hidden in the caldera floor. We conclude that the ~150 m thick mafic tephra and lava succession of the caldera walls is younger than 24 ka, and that major caldera subsidence occurred at ~6 ka. Masaya is thus a young volcano but has only produced frequent but low-intensity eruptions during the past ~1.5 ka (Walker et al., 1993). The three large caldera eruptions show an evolution to more evolved magma composition with time (Fig. 11B) but the more recent eruptive products span the entire compositional range.

Presently, there is no indication that Masaya will return to a more violent type of activity in the foreseeable future but little is known about how large basaltic eruptions announce themselves.

The Chiltepe volcanic complex had 6 highly explosive eruptions during the past ~17 ka, totaling at least 23 km<sup>3</sup> (Kutterolf et al., submitted for publication-b) of dacitic tephra, the last and largest (CT) occurring 1.9 ka ago. Active sulfurous fumaroles (own observations spring, 2006) at the NW Xiloà crater rim may indicate that the magmatic–hydrothermal system is still alive. Freundt et al. (2006a) showed that the variation of cumulative erupted magma-mass over time follows an exponential pattern (Fig. 11A) indicating an accelerating evolution of the system. The dacitic tephtras (excluding the compositionally distinct MaT) became less evolved with time (Fig. 11A). Since they erupted from different vents and reservoirs, this does not reflect repeated tapping of a long-lived compositionally zoned magma chamber. More likely, it seems that regional factors such as an extensional tectonic regime might have favored explosive eruptions of magmas in an increasingly less evolved state of chemical differentiation. Although the data is not conclusive in regard to the timing of the next eruption, we believe that its past evolution makes the Chiltepe volcanic complex the most likely candidate for the next big eruption in central Nicaragua.

However, we emphasize that our stratigraphic work (Fig. 7 in Freundt et al., 2006a) has shown that the Nejapa–Miraflores volcanic zone produced its last surtseyan eruption less than 1.8 ka ago (overlying the MT); such an eruption most probably will occur again in densely populated western Managua and might be even more hazardous than a Plinian eruption at Chiltepe.

### 8.2. Tephra dispersal and wind directions

The tephra succession investigated was largely produced by fallout from variably high subplinian to plinian eruption columns. The extent and direction of fallout dispersal depends on the direction and intensity of the winds and their vertical variations in the atmosphere.

Present-day wind conditions in Nicaragua are summarized as monthly averages in Fig. 12 by using the long-term data from the Climate Diagnostics Center (NOAA-CIRES, 2001) of the National Centers for Environmental Prediction (NCEP). Modern wind patterns indicate a constant stratospheric wind to the west above 27 km height that is strongest during the rainy season (May–October; Fig. 12). Lower tropospheric winds blow also mainly toward the west and northwest throughout the year. At the tropopause strong winds

occur toward the north and east during the dry season (November–April) while moderate winds blow toward the northwest and southwest during the rainy season.

Isopach patterns from eruptions of large inferred column heights (>27 km) vary between two extremes: the CT has a fairly straight distribution toward westerly directions from the vent, whereas the direction of the LAT first points to the northnorthwest and then bends to the west (Fig. 4C,G). Applying present-day wind directions to the last 24 ka, the pattern of the CT would be compatible with an eruption during the rainy season, July–September. In contrast, the LAT probably erupted during the dry season. As a note of caution it should be emphasized that all eruptions were multiphase events and that the isopachs for the tephra packages shown here thus do not reflect moderate changes in wind conditions during these eruptions. The dispersal patterns of the other tephtras investigated are also compatible with the modern wind profile. This compatibility is an indication, albeit no proof, that the wind pattern may indeed have remained approximately constant over the past 30 ka. Carey and Sigurdsson (2000) also observed that widespread tephtras deposited in the Caribbean record constant wind conditions, at least over the Quaternary. In their review of Quaternary climate changes, Rahmstorf and Sirocko (2004) concluded that the basic pattern of the meridional circulation cells of the atmosphere did not change, although there might have been changes in strength and some shift in latitudes.

### 8.3. Morphological evolution

Two major sections of the west-central Nicaraguan stratigraphic succession are marked by large regional unconformities. The unconformity with the largest amplitude (>50 m) formed >17 ka ago, separates the Mateare and Chiltepe formations in the region north of Mateare (U1 in Fig. 2), and extends onto the top of the escarpment of the Mateare Fault west of Mateare town (locality A127 in Fig. 4D). A younger ( $\leq 6$  ka) phase of erosion is evident from unconformities above each of the Xiloà and Mateare tephtras reaching several meters in amplitude (U2 and U3 in Fig. 2). Channels of the youngest erosional unconformity U3 are filled with thick fluvial volcaniclastic sediments whereas the detritus associated with the older unconformities appears to have been almost completely discharged into Lake Managua. South and west of the city of Managua, a regional unconformity of >10 m amplitude lies between the MTL–LCT and the SAT (U4 in Fig. 2), and is thus time-equivalent to the U2- and U3-unconformities in the north. However, there is no evidence of significant erosion south

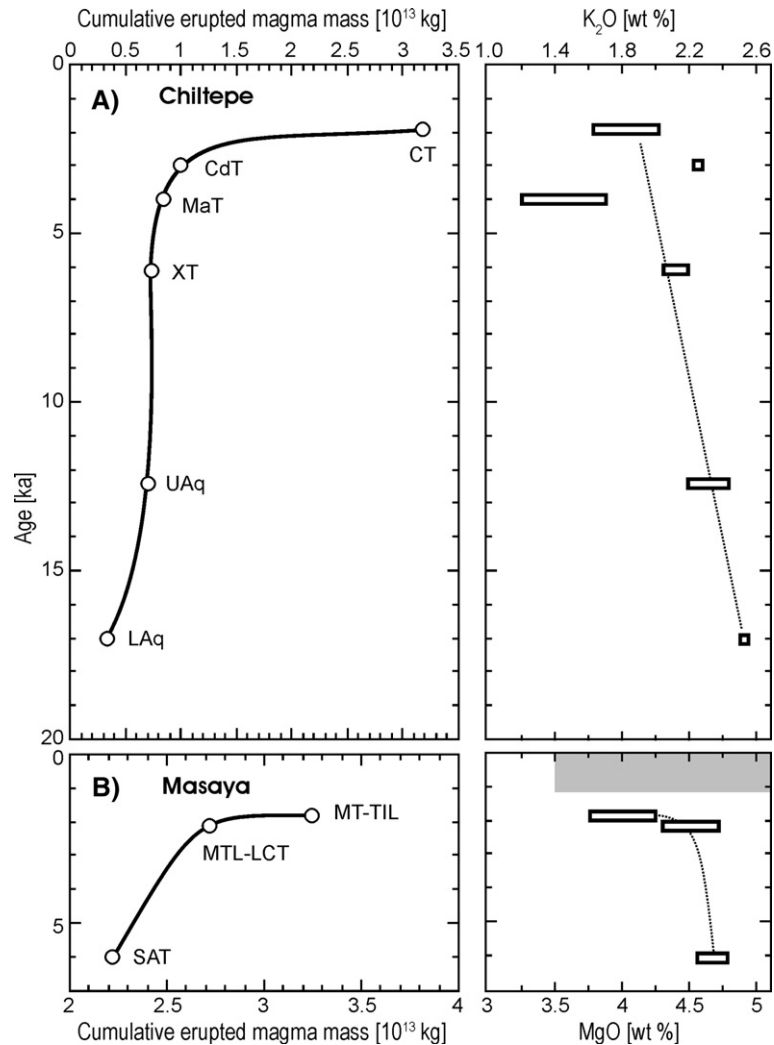


Fig. 11. (A) Cumulative mass of erupted magma versus eruption age (left panel) for the Chiltepe volcanic complex in comparison to bulk-rock potassium concentrations versus eruption age (right panel). Note that potassium content (degree of differentiation) decreases with time whereas magma eruption rate increases. The Mateare Tephra (MaT) is excluded from the dashed trend in the right panel because of its distinct low-K composition compared to the other dacites. (B) Cumulative mass of erupted magma versus eruption age for the Masaya Caldera mafic tephtras in comparison to magnesium contents versus eruption age. Data are insufficient to deduce an evolutionary trend. Gray bar indicates compositional range of younger, mostly intra-caldera eruption products (Walker et al., 1993).

of Managua that would correlate with the large U1-unconformity near Mateare. Intervals of the volcanic succession between and above these unconformities are conformably stratified except for rare, small erosional channels. In addition yellow weathered tuff layers with variably developed paleosols on top typically separate primary tephtras.

The U1-unconformity caps the conformably stratified, ~30 m thick upper section of the Mateare Formation. This succession is cut by numerous faults in the area where the Mateare Fault, the western boundary of the Nicaraguan Depression (Weinberg, 1992), approaches

Lake Managua and turns from an NNW–SSE to an NW–SE strike direction, as indicated by lake bathymetry. All these faults terminate at the large unconformity U1, suggesting that this tectonic activity ended during the transition from the Mateare to the Chiltepe formation at 17 ka. Therefore, the relief-forming U1-unconformity probably formed in response to tectonic activity (dextral transtension; Weinberg, 1992) at the Mateare Fault. We have found no evidence indicating that the second phase of erosion, marked by the U2 to U4 unconformities, was related to tectonic activity. Therefore the period 2.5–6 ka must have been a time of

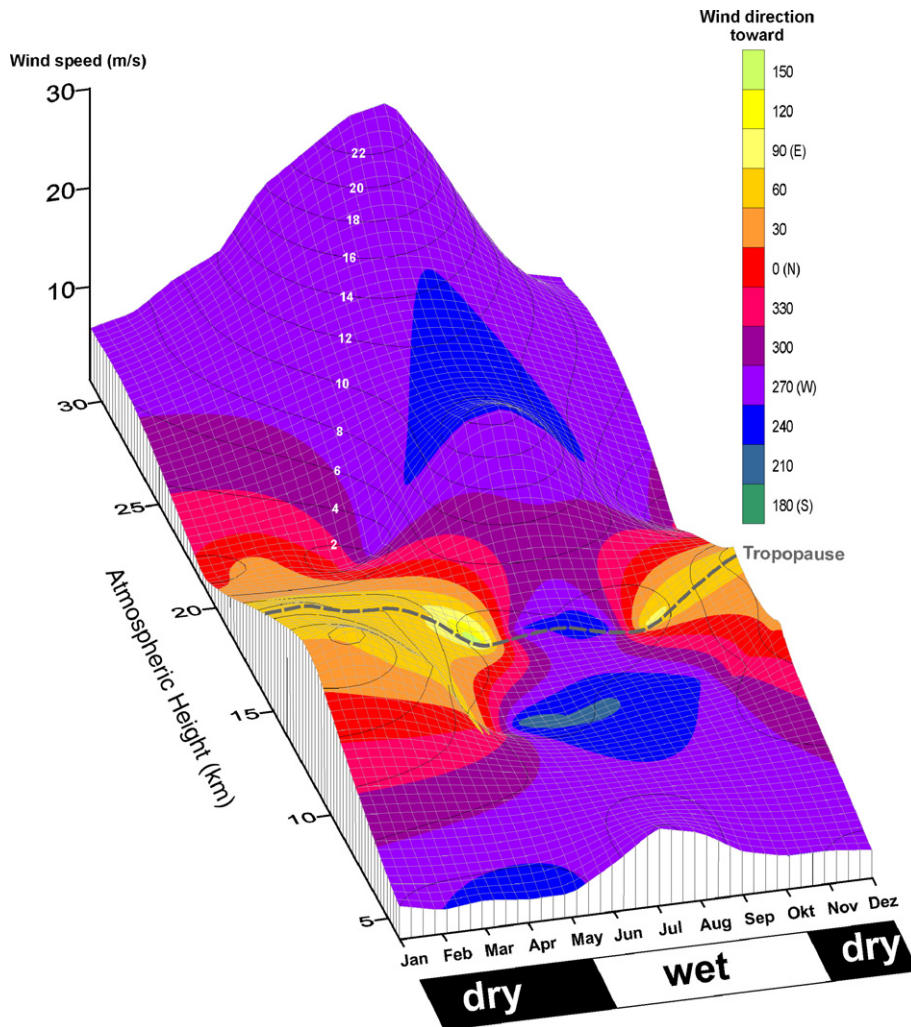


Fig. 12. Diagram of monthly averaged wind conditions in western Nicaragua based on the 20 years long-term climatic data set from the Climate Diagnostics Center (NOAA-CIRES, 2001) of the National Centres for Environmental Prediction (NCEP). Wind velocity ( $z$ -axis) varies with height in the atmosphere ( $y$ -axis) and with time through the year ( $x$ -axis). The color-coding specifies the wind directions which are particularly variable near the tropopause (dashed line at 16 km height) through the wet and dry seasons. White numbers give the strength of equal wind speed iso-lines (m/s).

enhanced precipitation during which repeated floods eroded deeply into the soft volcanoclastic deposits and locally emplaced fluvial sediments.

#### 8.4. Size of magmatic systems

Systematic changes in magma composition along the Central American Volcanic Arc (CAVA), were recognized in the early 80's and are the subject of continuing discussions (Stoiber and Carr, 1973; Carr, 1984; Feigenson and Carr, 1986; Patino et al., 2000; Carr et al., 2003; Feigenson et al., 2004; Carr et al., 2007). One aspect includes the correlation of chemical parameters and volcanic edifice volumes. Concentrations of LIL-elements (normalized to 52% silica) generally increase with

edifice volume (Carr, 1984) whereas the Ba/La ratio decreases (Carr et al., 1990). Edifice volume also increases with the spacing between volcanic centers (Carr, 1984). Edifice volume is considered to be a proxy for the size of the underlying magmatic system and associated to magma production rate (Carr, 1984; Carr et al., 2007). Carr and coworkers noted that this proxy suffers from considerable uncertainties, including poorly constrained age relationships, masses of intruded magma as well as of the mass of widely dispersed tephra. Our present data sheds some light on the latter.

Adding the 6 km<sup>3</sup> edifice volume of the Chiltepe complex given by Carr et al. (2003) to our volumes (30 km<sup>3</sup>) of the <17 ka tephra (LAq, UAq, XT, MaT, CdT, CT) on land as well as offshore (Kutterolf et al.,

submitted for publication-b), and converting it to magma mass by considering densities and pore spaces, yields 4 times the mass of the edifice alone. Analogously, the tephra from Apoyo Caldera make up 5 times the edifice volume. These numbers demonstrate that, in the case of silicic volcanoes, the size of the magmatic system is severely underestimated when approximated by the edifice volume alone while most of the erupted mass was distributed over huge areas.

## 9. Summary

We have newly identified and radiocarbon dated a number of widespread tephra in western Nicaragua and integrated them with previously described tephra into a stratigraphic framework. The isopach and isopleth maps of all tephra allowed to determine erupted volumes and eruption parameters.

The 9 dacitic to rhyolitic and 4 basaltic to andesitic highly explosive eruptions from mainly three volcanic complexes, Chiltepe, Masaya and Apoyo, we identified here, have produced a total volume of at least 37 km<sup>3</sup> of widespread tephra in west-central Nicaragua as well as at least 48 km<sup>3</sup> distally in the Pacific Ocean (Kutterolf et al., submitted for publication-b). The corresponding magma mass of 184 Gt was to 84% of evolved and to 16% of mafic composition. The overall long-term average magma mass flux contributing to highly explosive eruptions would have been about 120 kg/s but our stratigraphic and age data show that the evolution at each contributing volcano followed a non-linear path over time. The three volcanoes cover a representative range of explosive arc volcanism at subduction zones. The dacitic Chiltepe complex generated 6 plinian eruptions during the past ~ 17 ka. Increasing mass discharge and decreasing repose times indicate an accelerating evolution that makes Chiltepe a likely candidate for the next big eruption. The Masaya caldera generated 3 highly explosive basaltic eruptions since ~6 ka, the possible time of Caldera formation. Since ~1.8 ka, the volcano has only experienced frequent but low-scale activity mainly inside the caldera. The Apoyo caldera produced a large plinian double-eruption 24 ka ago and is obviously a volcano with very long repose times on the order of 10<sup>4</sup> years.

The plinian tephra studied here, both of evolved and mafic compositions, were emplaced from eruption columns penetrating variably high into the stratosphere, where prevailing winds caused dispersal into westerly directions. All these eruptions thus carried much of their exsolved volatiles into the stratosphere, and deposited much of their solid material into the Pacific Ocean.

The stratigraphic framework and the data on erupted masses and compositions forms a useful basis for future studies on the evolution of the magmatic systems, their volatile output into the atmosphere, and their eruption dynamics.

## Acknowledgements

We gratefully acknowledge the support by the Instituto Nicaragüense de Estudios Territoriales (INETER) in Managua, particularly by Dr. Wilfried Strauch and all the drivers who accompanied us during field work. WP acknowledges a PhD stipend by the Deutscher Akademischer Austauschdienst (DAAD). This publication is contribution no. 92 of the Sonderforschungsbereich 574 “Volatiles and Fluids in Subduction Zones” at Kiel University. We also appreciate the helpful comments and suggestions of Costanca Bonadonna, Claus Siebe and an anonymous person who reviewed this paper.

## Appendix A. Supplementary data

Supplementary data associated with this article can be found, in the online version, at [doi:10.1016/j.jvolgeores.2007.02.006](https://doi.org/10.1016/j.jvolgeores.2007.02.006).

## References

- Bice, D.C., 1985. Quaternary volcanic stratigraphy of Managua, Nicaragua: correlation and source assignment for multiple overlapping plinian deposits. *Geol. Soc. Amer. Bull.* 96, 553–566.
- Borgia, A., van Wyk de Vries, B., 2003. The volcano–tectonic evolution of Concepción, Nicaragua. *Bull. Volcanol.* 65, 248–266.
- Carey, S., Sigurdsson, H., 2000. Grain size of Miocene volcanic ash layers from Sites 998, 999, and 1000: implications for source areas and dispersal. In: Leckie, R.M., Sigurdsson, H., Acton, G.D., Draper, G. (Eds.), *Proceedings ODP. Scientific Results*, vol. 165, pp. 101–110.
- Carey, S., Sparks, R.S.J., 1986. Quantitative models of fallout and dispersal of tephra from volcanic eruption columns. *Bull. Volcanol.* 48, 109–125.
- Carr, M., Feigenson, M.D., Patino, L.C., Walker, J.A., 2003. Volcanism and geochemistry in Central America: progress and problems, inside the subduction factory. *AGU spec. pub. Geophysical Monograph*, vol. 138, pp. 153–174.
- Carr, M.J., 1984. Symmetrical and segmented variation of physical and geochemical characteristics of the Central American Volcanic Front. *J. Volcanol. Geotherm. Res.* 20, 231–252.
- Carr, M.J., Feigensohn, M.D., Benett, E.A., 1990. Incompatible element and isotopic evidence for tectonic control of source mixing and melt extraction along the central American arc. *Contrib. Mineral. Petrol.* 105, 369–380.
- Carr, M.J., Patino, L.C., Feigenson, M.D., 2007. Petrology and geochemistry of lavas. In: Buntschuh, J., Alvarado, G.E. (Eds.), *Central America—Geology, Resources and Hazards*, vol. 2. Balkema, Rotterdam, Netherlands, pp. 565–591.

- Cowan, H., Prentice, C., Pantosti, D., de Martini, P., Strauch, W., 2002. Late Holocene earthquakes on the Aeropuerto Fault, Managua, Nicaragua. *Bull. Seismol. Soc. Am.* 92, 1694–1707.
- Dengo, G., Bohnenberger, O., Bonis, S., 1970. Tectonics and volcanism along the Pacific Marginal Zone of Central America. *Geol. Rundsch.* 59, 1215–1232.
- Ehrenborg, J., 1996. A new stratigraphy for the Tertiary volcanic rocks of the Nicaraguan highland. *Geol. Soc. Amer. Bull.* 108, 830–842.
- Feigenson, M.D., Carr, M.J., 1986. Positively correlated Nd and Sr isotope ratios of lavas from the Central American volcanic front. *Geology* 14, 79–82.
- Feigenson, M.D., Carr, M.J., Maharaj, S.V., Bolge, L.L., Juliano, S., 2004. Lead isotope composition of Central American Volcanoes: influence of the Galapagos Plume. *Geochem. Geophys. Geosyst.* 5 (6), 1–14.
- Fierstein, J., Nathenson, M., 1992. Another look at the calculation of fallout tephra volumes. *Bull. Volcanol.* 54, 156–167.
- Freundt, A., Kutterolf, S., Schmincke, H.U., Hansteen, T.H., Wehrmann, H., Perez, W., Strauch, W., Navarro, M., 2006a. Volcanic hazards in Nicaragua: past, present, and future. In: Rose, W.I., Bluth, G.J.S., Carr, M.J., Ewert, J., Patino, L.C., Vallance, J.W. (Eds.), *Volcanic hazards in Central America*. *Geol. Soc. Am. Spec. Publ.*, pp. 141–165.
- Freundt, A., Kutterolf, S., Wehrmann, H., Schmincke, H.-U., Strauch, W., 2006b. Eruption of the dacite to andesite zoned Mateare Tephra, and associated tsunamis in Lake Managua, Nicaragua. *J. Volcanol. Geotherm. Res.* 149, 103–123.
- Girard, G., van Wyk de Vries, B., 2005. The Managua Graben and Las Sierras–Masaya volcanic complex (Nicaragua): pull-apart localization by an intrusive complex: results from analogue modeling. *J. Volcanol. Geotherm. Res.* 144, 37–57.
- Houghton, B.F., Wilson, C.J.N., Pyle, D.M., 2000. Pyroclastic fall deposits. In: Sigurdsson, H.e.a. (Ed.), *Encyclopedia of Volcanoes*. Academic Press, pp. 555–570.
- Hradecky, P., 2001. Informe Final de Consultoría para el Proyecto “Actualización del Mapa Geológico-estructural del Área de Managua” Instituto Nicaragüense de Estudios Territoriales (INETER), Managua.
- Krusi, A., Schultz, J., 1979. Base surge deposits of the Nicaraguan volcano Masaya (Abstr.). *Geol. Soc. Am. Abstr. Prog.* 11, 87–88.
- Kuang, S.J., 1971. Estudio Geológico del Pacífico de Nicaragua, Nicaragua Catastro e Inventario de Recursos Naturales.
- Kutterolf, S., Freundt, A., Pérez, W., Schmincke, H.U., submitted-a. The Pacific offshore record of Plinian arc volcanism in Central America, part 2: distal tephra from volcanoes in Guatemala and El Salvador, and along-arc eruption chronology. *Geochem. Geophys. Geosyst.*
- Kutterolf, S., Freundt, A., Schacht, U., Bürk, D., Harders, R., Mörz, T., Pérez, W., Wehrmann, H., Schmincke, H.-U., submitted-b. The Pacific offshore record of Plinian arc volcanism in Central America, part 1: the sources of tephra offshore Nicaragua, and implications for continental-slope geology. *Geochem. Geophys. Geosyst.*
- Kutterolf, S., Schacht, U., Wehrmann, H., Freundt, A., Mörz, T., 2007. Onshore to offshore tephrostratigraphy and marine ash layer diagenesis in Central America. In: Buntschuh, J., Alvarado, G.E. (Eds.), *Central America—Geology, Resources and Hazards*, vol. 2. Balkema, Lisse, Niederlande, Tokio, Japan, pp. 395–423.
- McBirney, A.R., 1955a. Thoughts on the eruption of the Nicaraguan Volcano Las Pilas. *Bull. Volcanologique, Series II*, vol. 17, pp. 113–117.
- McBirney, A.R., 1956. The Nicaraguan volcano Masaya and its caldera. *Trans. Am. Geophys. Union* 37, 83–96.
- McBirney, A.R., Williams, H., 1965. Volcanic history of Nicaragua. *Univ. Calif. Publ. Geol. Sci., Berkeley and Los Angeles*, vol. 55, 1–65 pp.
- NOAA-CIRES, 2001. Data provided from NCEP wind-data. Climate Diagnostics center (NOAA-CIRES), Boulder, Colorado <http://www.cdc.noaa.gov/cgi-bin/DataMenus.pl?dataset=NCEP>.
- Paladio-Melosantos, L.O., Solidum, R.U., Scott, W.E., Quiambao, R.B., Umbal, J.V., Rofodolfo, K.S., Tubianosa, B.S., Reyes, P.J.D., Alonso, R.A., Ruelo, H.B. (Eds.), 1996. Tephra Falls of the 1991 eruptions of Mount Pinatubo. Fire and Mud: Eruptions and Lahars of Mount Pinatubo, Philippines. USGS, Hong Kong, pp. 325–332.
- Patino, L.C., Carr, M., Feigenson, M.D., 2000. Local and regional variations in Central American arc lavas controlled by variations in subducted sediment input. *Contrib. Mineral. Petrol.* 138, 256–283.
- Perez, W., 2007. Basaltic Plinian and violent Surtseyan eruptions from Masaya Caldera, Nicaragua. PhD Thesis, University of Kiel, 194 pp.
- Pérez, W., Freundt, A., 2006. The youngest highly explosive basaltic eruptions from Masaya Caldera (Nicaragua): stratigraphy and hazard assessment. In: Rose, W.I., Bluth, G.J.S., Carr, M.J., Ewert, J., Patino, L.C., Vallance, J.W. (Eds.), *Volcanic Hazards in Central America*. *Geol. Soc. Am. Spec. Publ.*, pp. 189–207.
- Pyle, D.M., 1989. The thickness, volume and grain size of tephra fall deposits. *Bull. Volcanol.* 51, 1–15.
- Rahmstorf, S., Sirocko, F., 2004. Modes of oceanic and atmospheric circulation during the Quaternary. *Earth System Analysis for Sustainability*, Berlin, Germany, pp. 129–142.
- Sapper, C., 1925. *Los Volcanes de America Central*, vol. 116. Max Niemeyer, Halle, Germany.
- Sebesta, J., 1997. Dynamic development of the relief in the Managua are, Nicaragua. *Acta Univ. Carol. Geogr.* 2, 93–109.
- Stoiber, R.E., Carr, M.J., 1973. Quaternary volcanic and tectonic segmentation of Central America. *Bull. Volcanol.* 37, 304–325.
- Stuiver, M., Polach, H.A., 1977. Discussion: reporting of  $^{14}\text{C}$  data. *Radiocarbon* 19, 355–363.
- Sussman, D., 1985. Apoyo Caldera, Nicaragua: a major Quaternary silicic eruptive center. *J. Volcanol. Geotherm. Res.* 24, 249–282.
- Ui, T., 1972. Recent volcanism in Masaya–Granada area, Nicaragua. *Bull. Volcanol.* 36, 174–190.
- Van Wyk de Vries, B., 1993. Tectonics and magma evolution of Nicaraguan volcanic systems. Doctoral Thesis. Open University, Milton Keynes, 328 pp.
- Walker, J.A., 1984. Volcanic rocks from the Nejapa and Granada cinder cone alignments, Nicaragua, Central America. *J. Petrol.* 25, 299–342.
- Walker, J.A., Williams, S.N., Kalamarides, R.I., Feigensohn, M.D., 1993. Shallow open-system evolution of basaltic magma beneath a subduction zone volcano: the Masaya caldera complex, Nicaragua. *J. Volcanol. Geotherm. Res.* 56, 379–400.
- Wehrmann, H., Bonadonna, C., Freundt, A., Houghton, B.F., Kutterolf, S., 2006. Fontana Tephra: a basaltic plinian eruption in Nicaragua. In: Rose, W.I., Bluth, G.J.S., Carr, M.J., Ewert, J., Patino, L.C., Vallance, J.W. (Eds.), *Volcanic Hazards in Central America*. *Geol. Soc. Am. Spec. Publ.*, pp. 209–223.
- Weinberg, R.F., 1992. Neotectonic development of western Nicaragua. *Tectonics* 11, 1010–1017.
- Weyl, R., 1980. Geology of Central America, In: Bender, F.e.a. (Ed.), *Beiträge zur Regionalen Geologie der Erdepp.*, 2nd ed. Gebr. Borntraeger, Berlin-Stuttgart, p. 371.
- Williams, S.N., 1952a. Geologic observations on the ancient human footprints near Managua, Nicaragua. *Contrib. Am. Anthro. A. Hist.* 52, 5–31.
- Williams, S.N., 1972. The geology of western Nicaragua. Tax Improvement and Natural Resource Inventory Project, Managua, Nicaragua, vol. 4.

- Williams, S.N., 1983a. Geology and eruptive mechanisms of Masaya Caldera Complex, Nicaragua. Unpubl. PhD thesis Thesis, Dartmouth College. Hanover, New Hampshire, USA, 169 pp.
- Williams, S.N., 1983b. Plinian airfall deposits of basaltic composition. *Geology* 11, 211–214.
- Wilson, L., Walker, G.P.L., 1987. Explosive volcanic eruptions-VI. Ejecta dispersal in plinian eruptions: the control of eruption conditions and atmospheric properties. *Geophys. J. R. Astron. Soc.* 89, 657–679.
- Woods, A.W., 1988. The fluid dynamics and thermodynamics of eruption columns. *Bull. Volcanol.* 50, 169–193.
- Zúñiga, A., Su, M., Sánchez, M., 2003. Thermal Manifestations in Nicaragua. *GHC Bulletin*, pp. 23–25. 9/2003.